Electronic Supplementary Information

A chiral binaphthyl-based coordination polymer as an enantioselective fluorescence sensor

Table of contents

Experimental

General experimental

All chemicals and solvents were used as obtained and without further purification. 4,4′-Dibromo-2,2′-binaphthol,[1] and $Pd(PPh_3)_4$,[2] were synthesised according to literature procedures. Fourier Transform Infrared spectra were measured on an ATR Bruker Alpha spectrometer between 4000 – 400 cm^{-1} with 4 cm^{-1} resolution and 32 scans and normalised as absorbance spectra. Thermal gravimetric analysis (TGA) was conducted on a Mettler Toledo TGA/SDTA851 instrument using aluminium crucibles as sample holders under high purity nitrogen. Typical analysis involved heating the sample up to 450 °C with a temperature increment of 5 °C/min^{-1}. Microanalysis was carried out at the Chemical Analysis Facility – Elemental Analysis Service in the Department of Chemistry and Biomolecular Science at Macquarie University, Australia. Powder diffraction data were collected on an XtaLAB Synergy diffractometer employing CuKα at λ = 1.5418 Å. PXRD patterns from single crystal structures were calculated using Mercury v.4.0. Absorption and emission experiments were performed with quartz cuvettes containing suspensions in acetonitrile; UV/vis absorption spectra were recorded on an Agilent Cary 60 UV-Vis spectrophotometer, and fluorescence spectra were recorded on an Agilent Cary Eclipse Fluorescence spectrophotometer.

Crystallography

Single crystal X-ray diffraction data was collected on the MX1 beamline at the Australian Synchrotron.[3] The single crystals of $[Zn_3(L1)(tma)_2(DMF)_3]\cdot 2DMF$ were transferred directly from the mother liquor into immersion oil and placed under a stream of nitrogen at 100 K. The crystal structure was solved by direct methods using the program SHELXT,[4] and refined using a full matrix least-squares procedure based on F^2 (SHELXL),[5] within the Olex2 GUI program.[6] Some disordered solvent molecules could not be satisfactorily modelled, hence the solvent mask routine with the Olex2 GUI was used. In the crystal analysis, a racemic sample of $[Zn_3(L1)(tma)_2(DMF)_3]\cdot 2DMF$ was analysed, resulting in the centrosymmetric space group of $P2_1/c$. Attempts to grow suitable single crystals of appropriate diffraction quality of enantiopure $[Zn_3((S)\text{-}L1)(tma)_2(DMF)_3]\cdot 2DMF$ were unsuccessful, resulting in smearing and weak diffraction at high angles even on synchrotron x-ray sources.

Fluorescence quenching experiments

Crystals of compound **(*S*)-1** were washed with acetonitrile and air-dried, then manually crushed in a mortar and pestle and suspended in acetonitrile (10 mL) at an effective concentration of 5×10^{-4} M. PXRD analysis indicates that samples of **1** retain their crystallinity after crushing. Small 0.5 mL aliquots of the 5×10^{-4} M stock solution were then further diluted with acetonitrile (24.5 mL) to yield stock suspensions at an effective concentration of 1×10^{-5} M. All suspensions were sonicated for a minimum

of 10 minutes to ensure even dispersion of particulates. Stock suspensions were stored away from direct sources of light.

The 5×10^{-4} M stock suspension was used for UV/vis absorption experiments. For recording of fluorescence spectra, 3 mL of the 1×10^{-5} M stock suspension of **(*S*)-1** was dispensed into a quartz cuvette. Spectrophotometer excitation wavelength was set to 229 nm, with a UV29 filter inserted to eliminate second and third harmonic signals. Chiral analytes were prepared as acetonitrile solutions at 3 mM, then added to the cuvette in increments of 10–500 µL until total analyte concentration in the cell reached 0.5 mM. Fluorescence spectra were recorded after each incremental addition of the analyte, with measurements consistently taken four minutes apart. Control experiments indicated suspensions of **(*S*)-1** were stable over this time period. Samples in the cuvette were shaken between fluorescence measurements to maintain an even dispersion of **(*S*)-1** within the suspension.

In the case of the amino acid methyl ester hydrochlorides, analytes were added to suspensions of **(*S*)-1** up to 24 hours prior to fluorescence measurements to allow enough time for chiral guest molecules to diffuse into the pores of the framework. This method resulted in closer agreement with quadratic Stern-Volmer behaviour.

Stern-Volmer analysis was conducted by plotting the fluorescence intensity of the 415 nm peak in each emission spectrum against the increasing concentration of chiral analytes. Enantioselectivity ratios were calculated by approximating the gradient of the linear fit for each quenching plot to the Stern-Volmer constant K_{SV}, as specified in the main text. Calibration experiments with Mosher's acid were conducted with racemic samples of the analyte at a total concentration of 0.3 mM within the cuvette. Three linear calibration plots were generated, then averaged by calculating the mean fluorescence intensity at each **ee** value. Error bars represent the highest standard deviation observed for the mean fluorescence intensity. 'Unknown' samples of Mosher's acid were prepared at a known **ee**, then added to suspensions of **(*S*)-1** as normal so that the resulting fluorescence intensity could be inserted into the equation of the linear fit for the calibration plot to yield a new **ee** value with less than 10% error.

Synthetic procedures

Synthesis of (*S*)-4,4′-dibromo-2,2′-diethoxy-1,1′-binaphthalene.

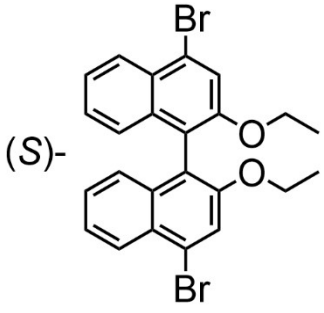

(*S*)-4,4′-Dibromo-1,1′-bi-2-napthol (0.370 g, 0.83 mmol), bromoethane (0.371 mL, 5.00 mmol), NaI (0.019 g, 0.13 mmol), and K_2CO_3 (0.576 g, 4.17 mmol) were suspended in acetone and heated at reflux for 18 hours. The reaction mixture was filtered, then the filtrate concentrated under reduced pressure. The oily residue was washed with hexane (2 mL) to give the product as an orange powder (0.35 g, 84%). ^{1}H NMR (400 MHz, $CDCl_3$) δ 8.23 (d, 2H, J = 8.8 Hz), 7.73 (s, 2H), 7.43-7.39 (m, 2H), 7.24-7.22 (m, 2H), 7.10 (d, 2H, J = 8.4 Hz), 4.08-4.00 (m, 4H), 1.07 (t, 6H, J = 6.8 Hz) ppm.

Synthesis of (*S*)-4,4′-dipyridyl-2,2′-diethoxy-1,1′-binaphthalene ((*S*)-L1).

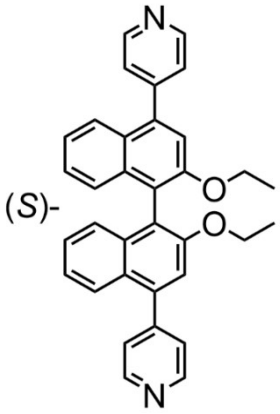

A suspension of (*S*)-4,4′-dibromo-2,2′-diethoxy-1,1′-binapthalene (0.32 g, 0.62 mmol), pyridyl-4-boronic acid (0.23 g, 1.86 mmol), $Pd(PPh_3)_4$ (45.0 mg, 0.039 mmol), and K_2CO_3 (0.43 g, 3.10 mmol) in 1,4-dioxane (12.5 mL) and H_2O (1.25 mL) was degassed under N_2 and heated to reflux for 16 hours. The solvent was removed under reduced pressure to give a red residue, which was partitioned between H_2O (30 mL) and CH_2Cl_2 (30 mL). The aqueous layer was extracted with CH_2Cl_2 (3 × 20 mL), then the combined organic layers were dried over $MgSO_4$, filtered and the solvent removed under reduced pressure to yield a dark red oil. The crude product was purified by column chromatography (gradient EtOAc, 5% Et_3N → 1% MeOH, EtOAc, 5% Et_3N) to yield the product as a yellow solid (0.31 g, 97%). ^{1}H NMR (400 MHz, $CDCl_3$) δ 8.85 (br s, 4H), 7.86 (d, J = 8.0 Hz, 2H), 7.62 (br s, 4H), 7.39 (s, 2H), 7.37 – 7.15 (m, 6H), 4.23 – 4.00 (m, 4H), 1.14 (t, J = 7.0 Hz, 6H) ppm. ^{13}C{^{1}H} NMR (101 MHz, $CDCl_3$) δ 153.8, 149.9, 148.9, 138.8, 134.7, 126.7, 126.6, 126.1, 125.4, 124.3, 121.0, 116.7, 65.4, 15.1 ppm. HRMS (ESI) m/z: $[M+H^+]^+$ calcd for $[C_{34}H_{28}N_2O_2]^+$,497.2229; found, 497.2417.

Synthesis of $[Zn_3((S)\text{-L1})(tma)_2(DMF)_3]\cdot 2DMF$ ((*S*)-1). A mixture of **(*S*)-L1** (14.8 mg, 0.030 mmol), $Zn(NO_3)_2\cdot 6H_2O$ (17.8 mg, 0.060 mmol), and trimesic acid (12.6 mg, 0.060 mmol) in DMF (6.0 mL) was heated at 85 °C for four days. The reaction mixture was cooled to room temperature before being washed with water and DMF, then filtered and dried to afford yellow block crystals of **(*S*)-L1** (9.3 mg, 21%). IR (ATR): 3070, 2975, 2926, 1669, 1623, 1585, 1498, 1422, 1339, 1212, 1189, 1148, 1096, 1061, 1030, 936, 843, 816, 765, 725, 673, 610, 567, 468, 437 cm^{-1}. Elemental analysis (%): calc'd for $[Zn_3C_{61}H_{55}N_5O_{17}]\cdot 2DMF$: C 54.88, H 4.74, N 6.69; found: C 54.51, H 4.67, N 6.95.

Table S1. Crystallographic parameters and structural refinement details for compound **1**.

Compound 1	$[Zn_3(\mathbf{L1})(tma)_2(DMF)_3]\cdot 2DMF$ (**1**)
Formula	$C_{67}H_{69}N_7O_{19}Zn_3$
M/g mol^{-1}	1472.40
Temperature (K)	100(2)
Crystal system	Monoclinic
Space Group	$P2_1/c$
Crystal size (mm^3)	0.1 × 0.06 × 0.05
Crystal Colour	Yellow
Crystal Habit	Block
a (Å)	25.909(5)
b (Å)	17.361(4)
c (Å)	17.014(3)
α (°)	90
β (°)	93.90(3)
γ (°)	90
V (Å^3)	7635(3)
Z	4
ρ_{calc} (g/cm^3)	1.281
μ (mm^{-1})	1.003
F(000)	3048.0
Radiation	Synchrotron (λ = 0.71073)
2Θ range for data collection (°)	1.576 to 58.882
Index ranges	$-31 \le h \le 31$, $-21 \le k \le 21$, $-22 \le l \le 22$
Reflections collected	96056
Independent reflections	16480 [R_{int} = 0.1112, R_{sigma} = 0.0701]
Data/restraints/parameters	16480/582/850
Goodness-of-fit on F^2	1.243
Final R indexes [I>=2σ (I)]	R_1 = 0.1233, wR_2 = 0.3174
Final R indexes [all data]	R_1 = 0.1984, wR_2 = 0.3922
Largest diff. peak/hole (e$^-$Å^{-3})	1.17/−1.72

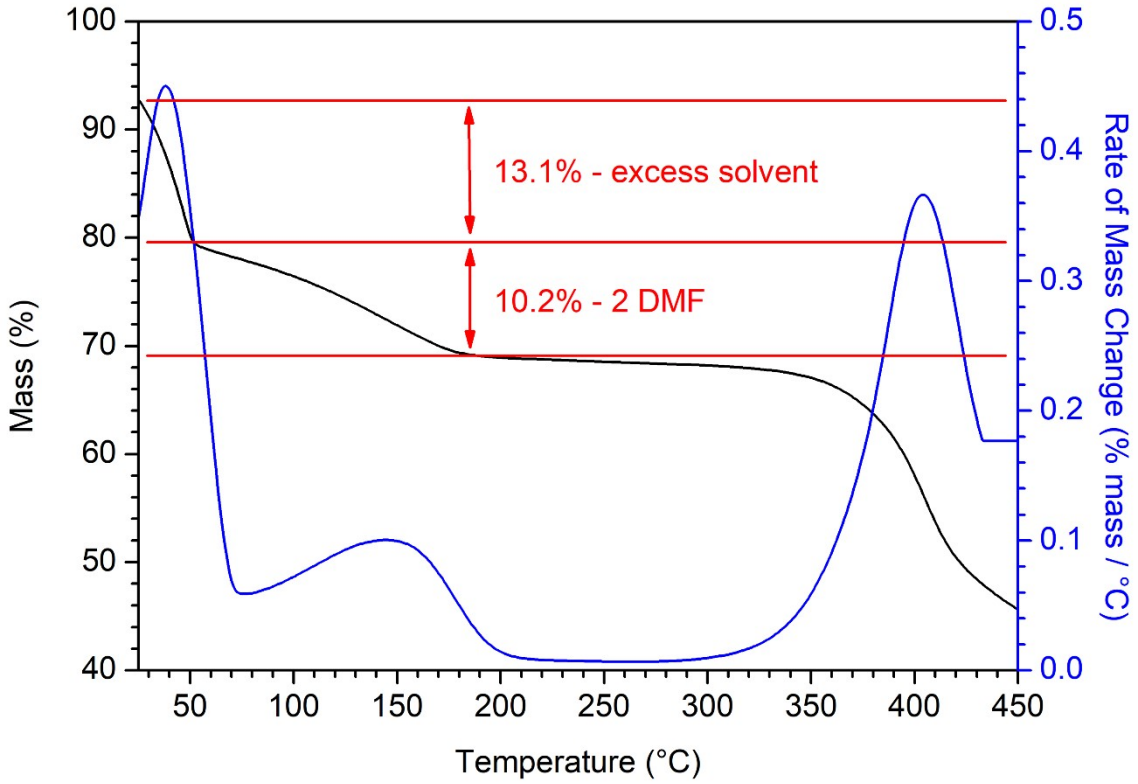

Figure S1. Thermal Gravimetric Analysis (TGA) of $[Zn_3(\mathbf{L1})(tma)_2(DMF)_3]\cdot 2DMF$ (**1**) from 25–450 °C, heated at a rate of 5 °C/min under nitrogen. The percentage mass loss is shown in black, and the rate of mass change is shown in blue. Mass losses assigned to individual molecules are approximate.

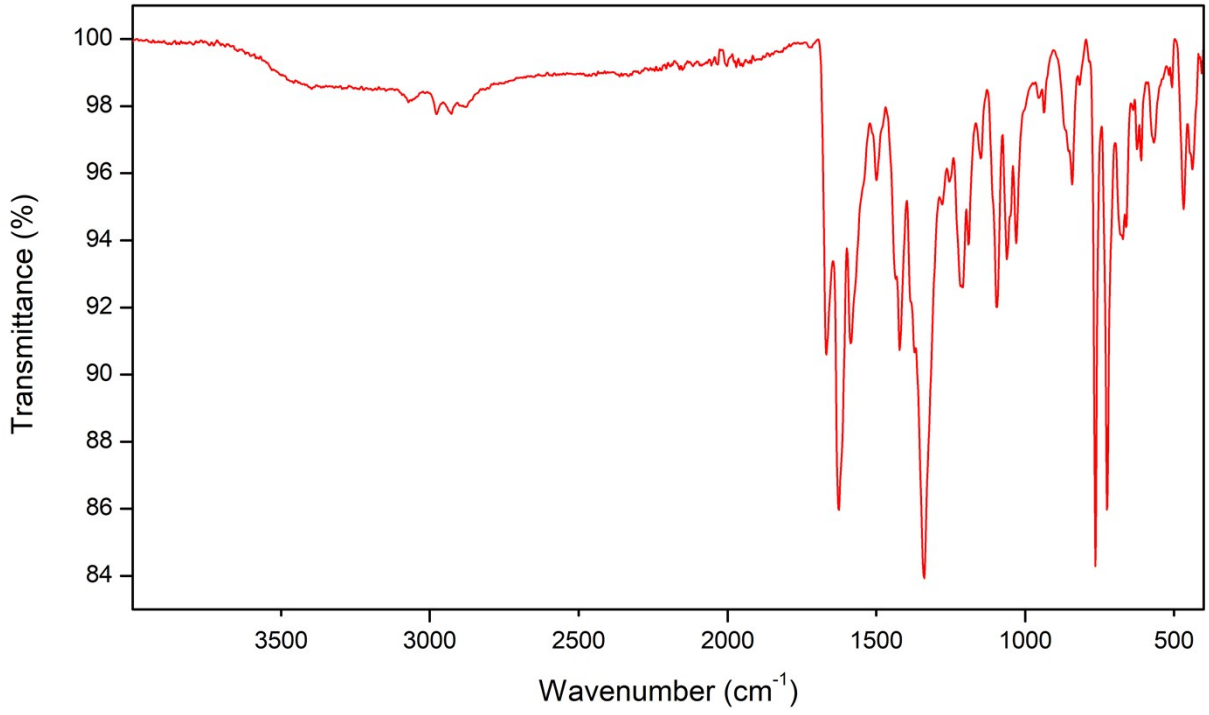

Figure S2. ATR infrared spectrum of $[Zn_3(\mathbf{L1})(tma)_2(DMF)_3]\cdot 2DMF$ (**1**) from 4000–400 cm^{-1}.

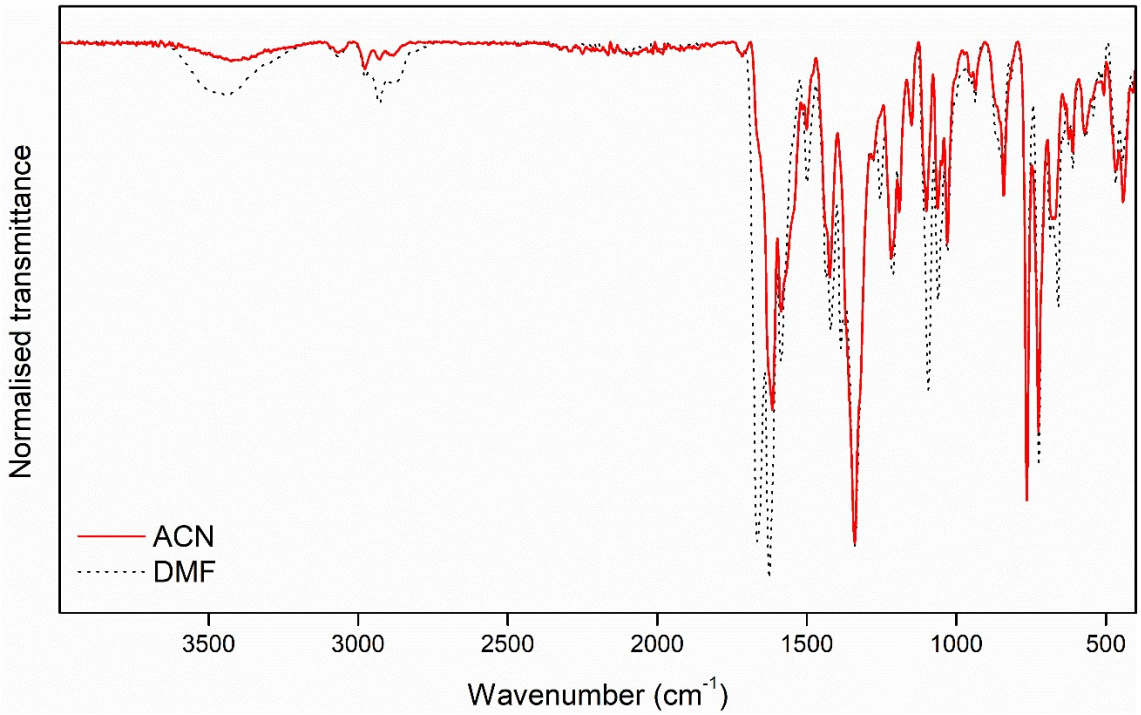

Figure S3. ATR infrared spectra of compound **(*S*)-1** from 4000–400 cm^{-1} before (black) and after (red) immersion in ACN. The relative weakening of the strong band at 1615–1625 cm^{-1} after immersion in ACN suggests the removal of DMF solvent molecules from within the channels of **(*S*)-1**.

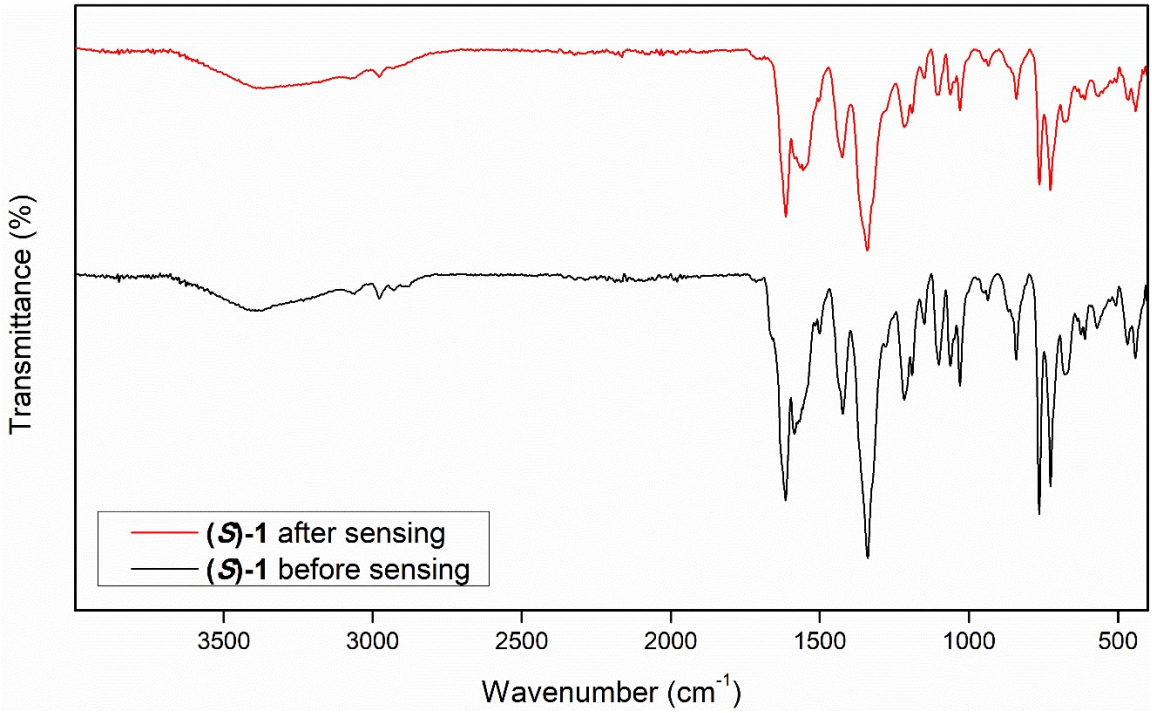

Figure S4. ATR infrared spectra of compound **(*S*)-1** from 4000–400 cm^{-1} before (black) and after (red) immersion in an ACN solution of Mosher's acid at a concentration of 0.43 mM, comparable to that used in fluorescence sensing experiments. Subtle changes such as the slight redshift of the strong bands in the 1700–1500 cm^{-1} region suggest successful guest incorporation within **(*S*)-1**.

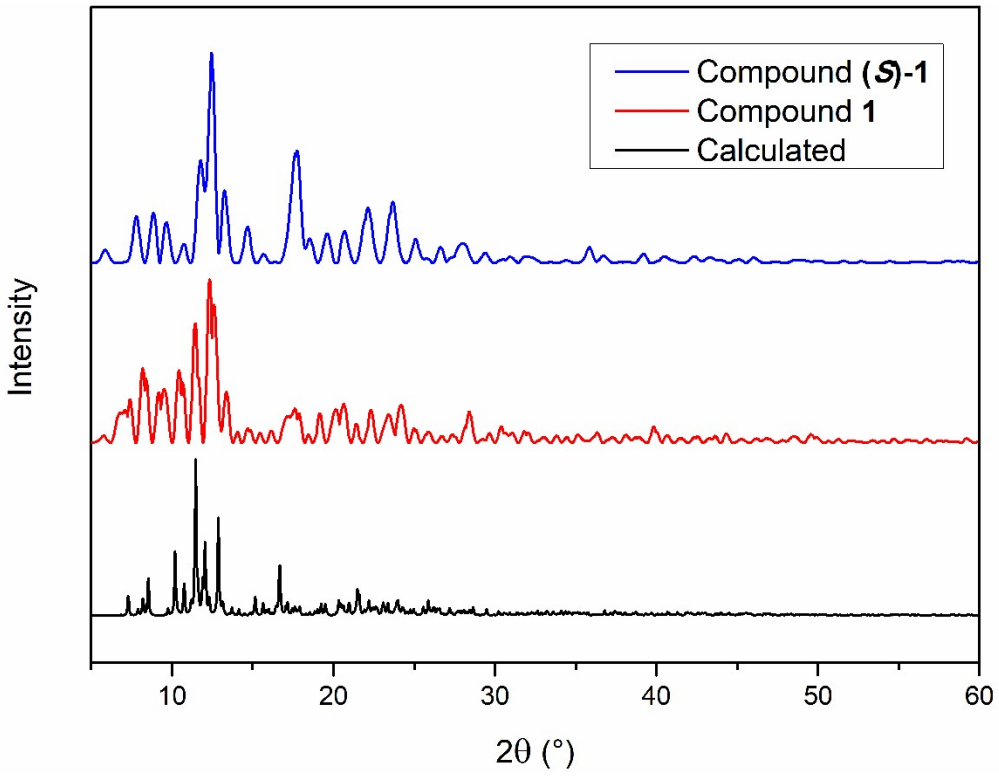

Figure S5. Calculated (black) vs. experimental PXRD patterns for racemic compound **1** (red) and enantiopure compound **(*S*)-1** (blue).

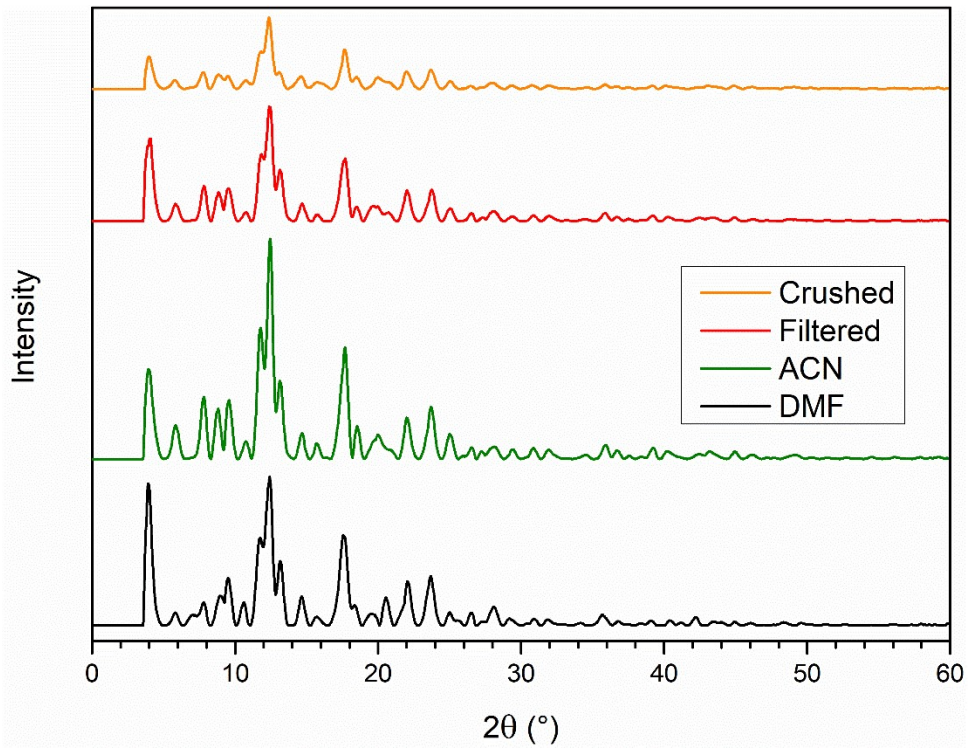

Figure S6. PXRD patterns of compound **1** measured for different samples: crystals from supernatant (black), crystals soaked in acetonitrile (green), crystals filtered and washed (red), and crystals crushed in a mortar and pestle (orange).

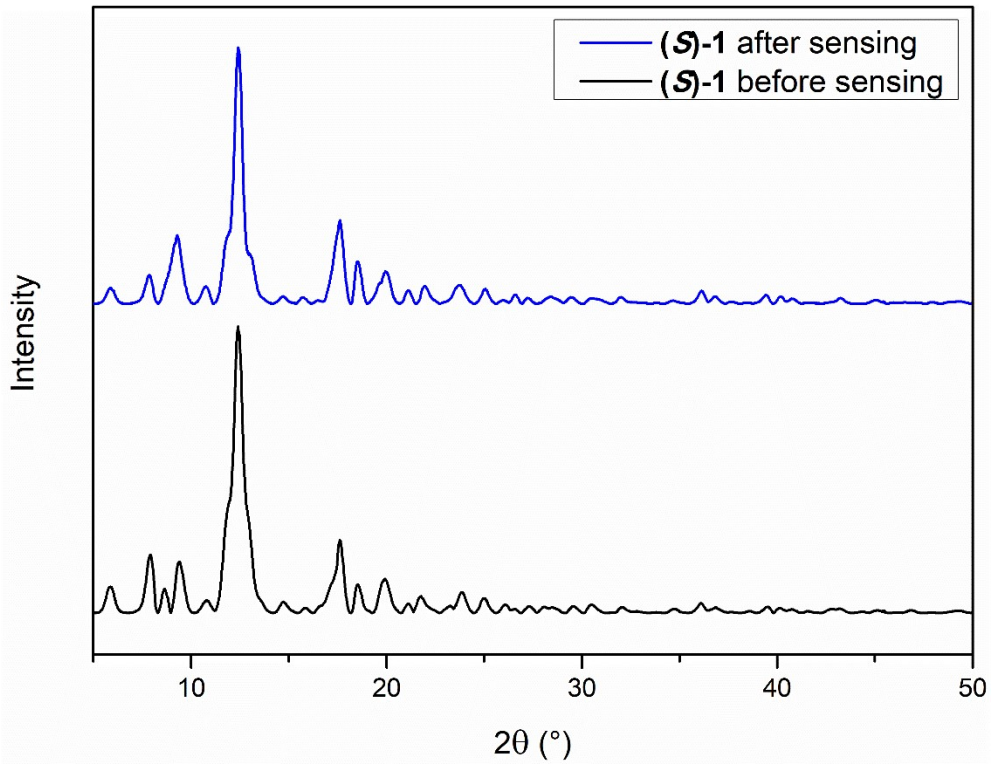

Figure S7. PXRD patterns of compound **(*S*)-1** before (black) and after (blue) immersion in an ACN solution of Mosher's acid at a concentration of 0.43 mM, comparable to that used in fluorescence sensing experiments.

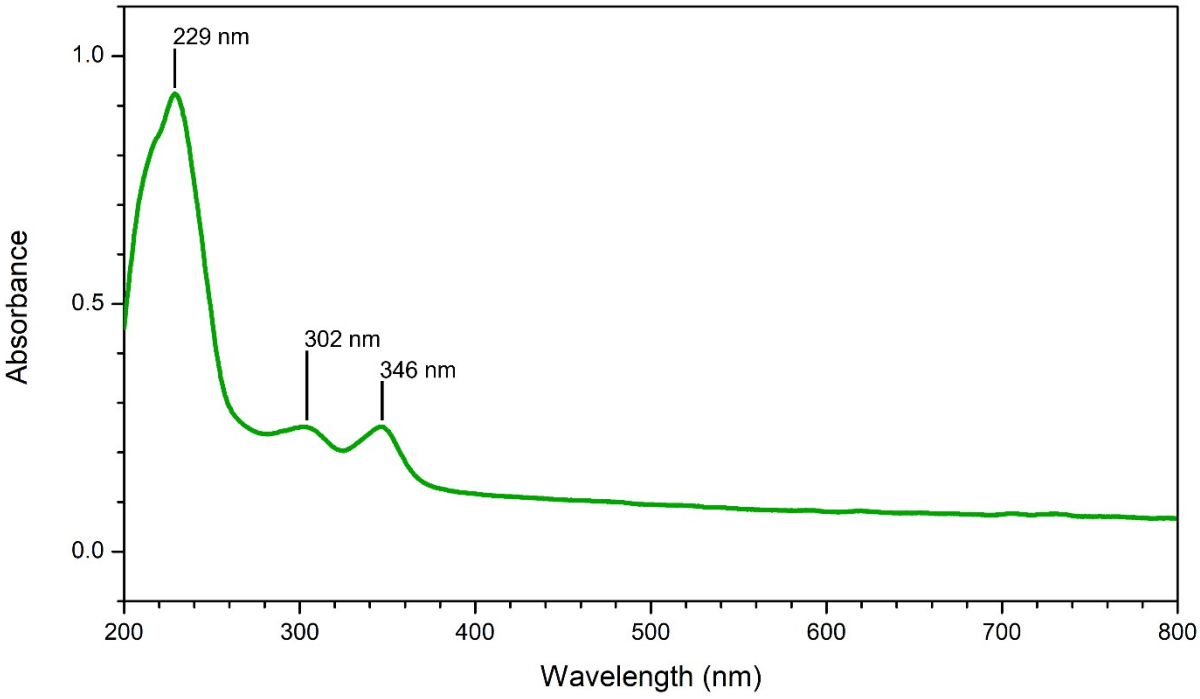

Figure S8. Normalised UV/vis absorption spectrum of compound **1** as a suspension in acetonitrile.

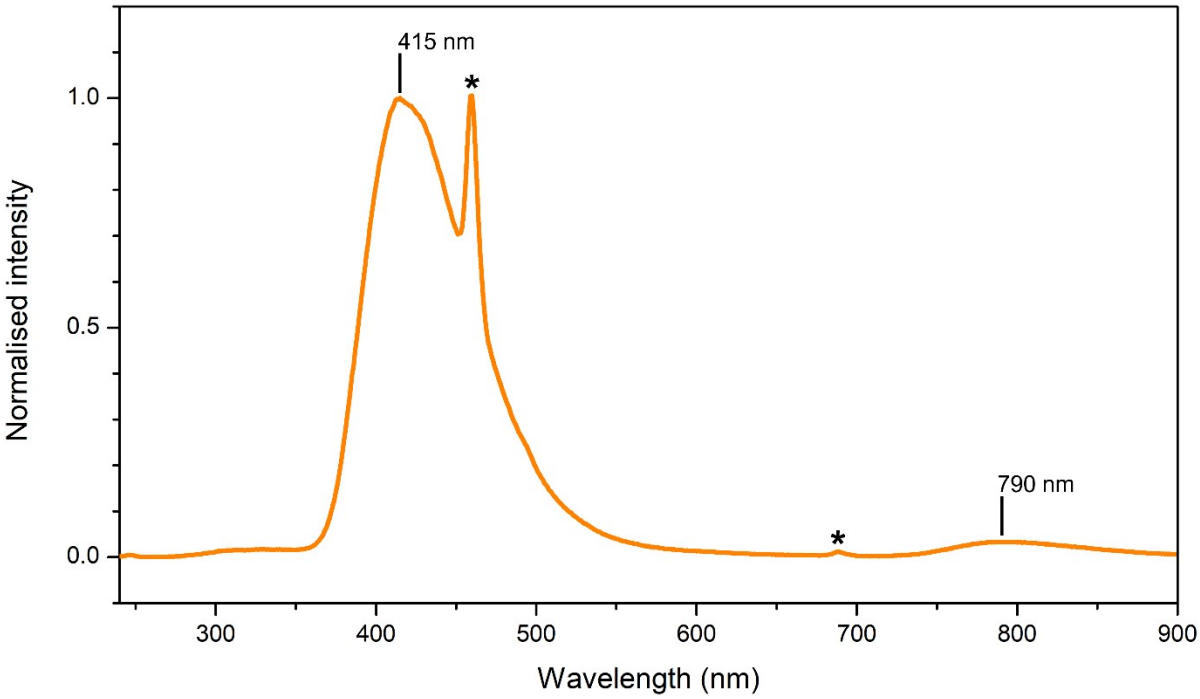

Figure S9. Normalised emission spectrum of compound **1** upon excitation at 229 nm as a suspension in acetonitrile. The peaks related to the second and third harmonics are indicated with asterisks.

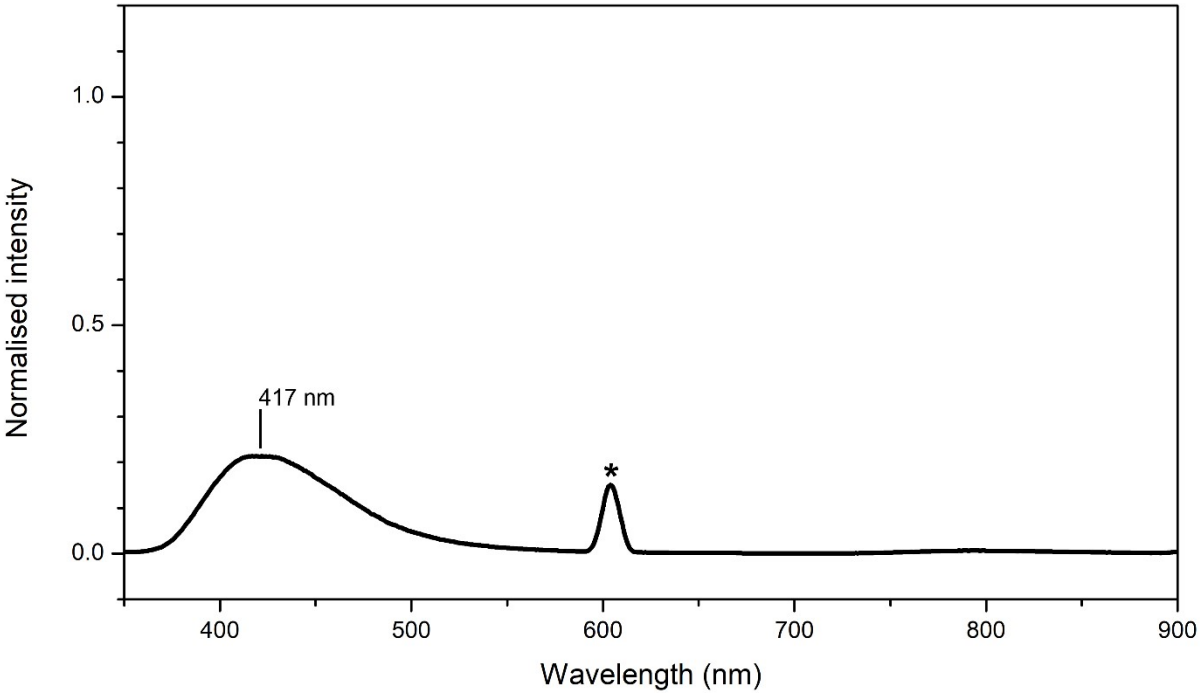

Figure S10. Normalised emission spectrum (relative to the intensity of the 415 nm peak in **Figure S9**) of compound **1** upon excitation at 302 nm as a suspension in acetonitrile. The peak related to the second harmonic is indicated with an asterisk.

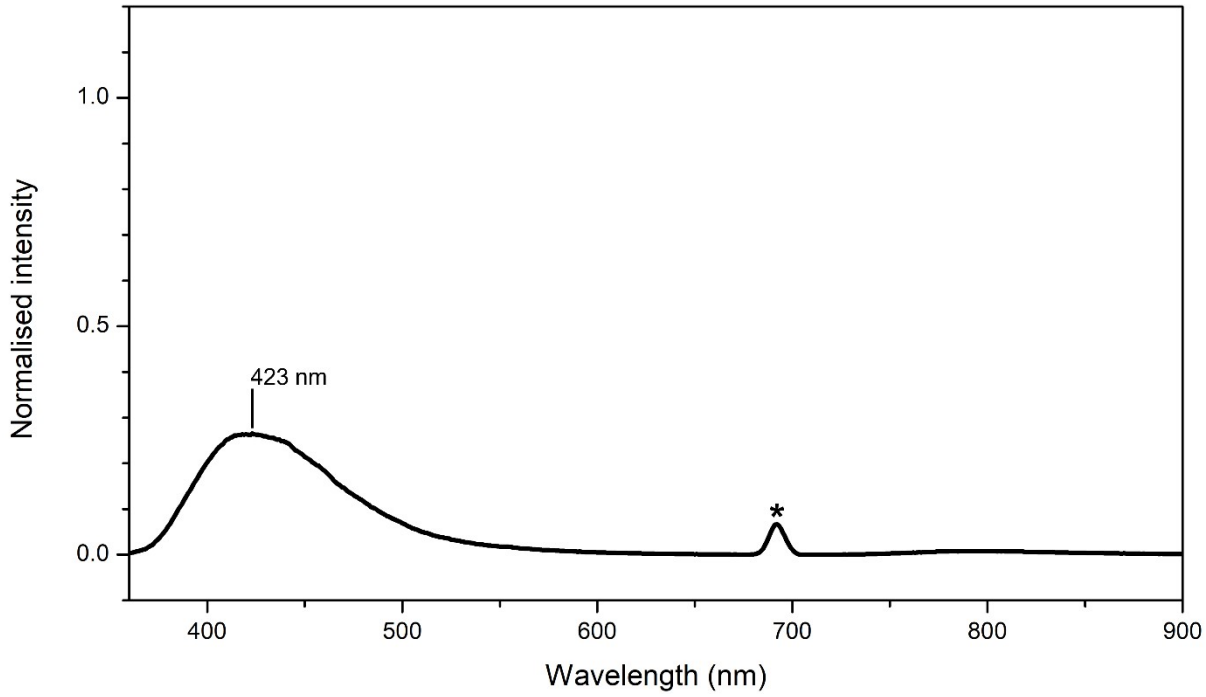

Figure S11. Normalised emission spectrum (relative to the intensity of the 415 nm peak in **Figure S9**) of compound **1** upon excitation at 346 nm as a suspension in acetonitrile. The peak related to the second harmonic is indicated with an asterisk.

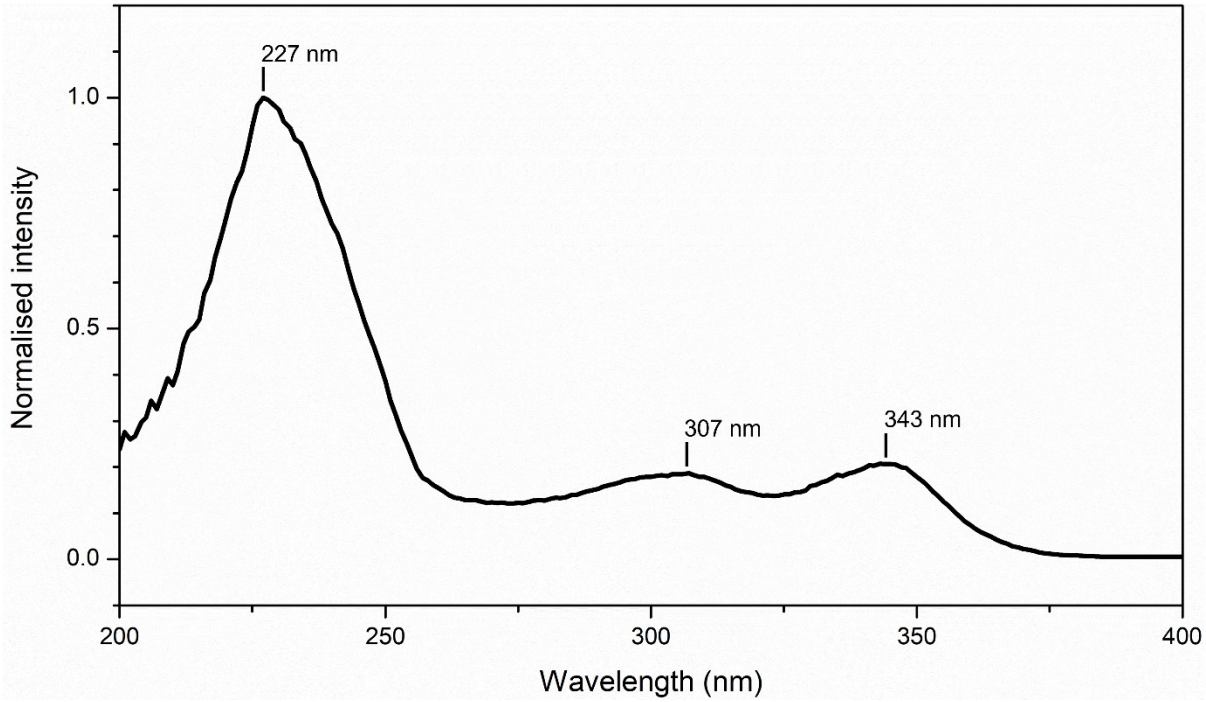

Figure S12. Normalised excitation spectrum of compound **(*S*)-1** as a suspension in acetonitrile, monitoring emission at 415 nm.

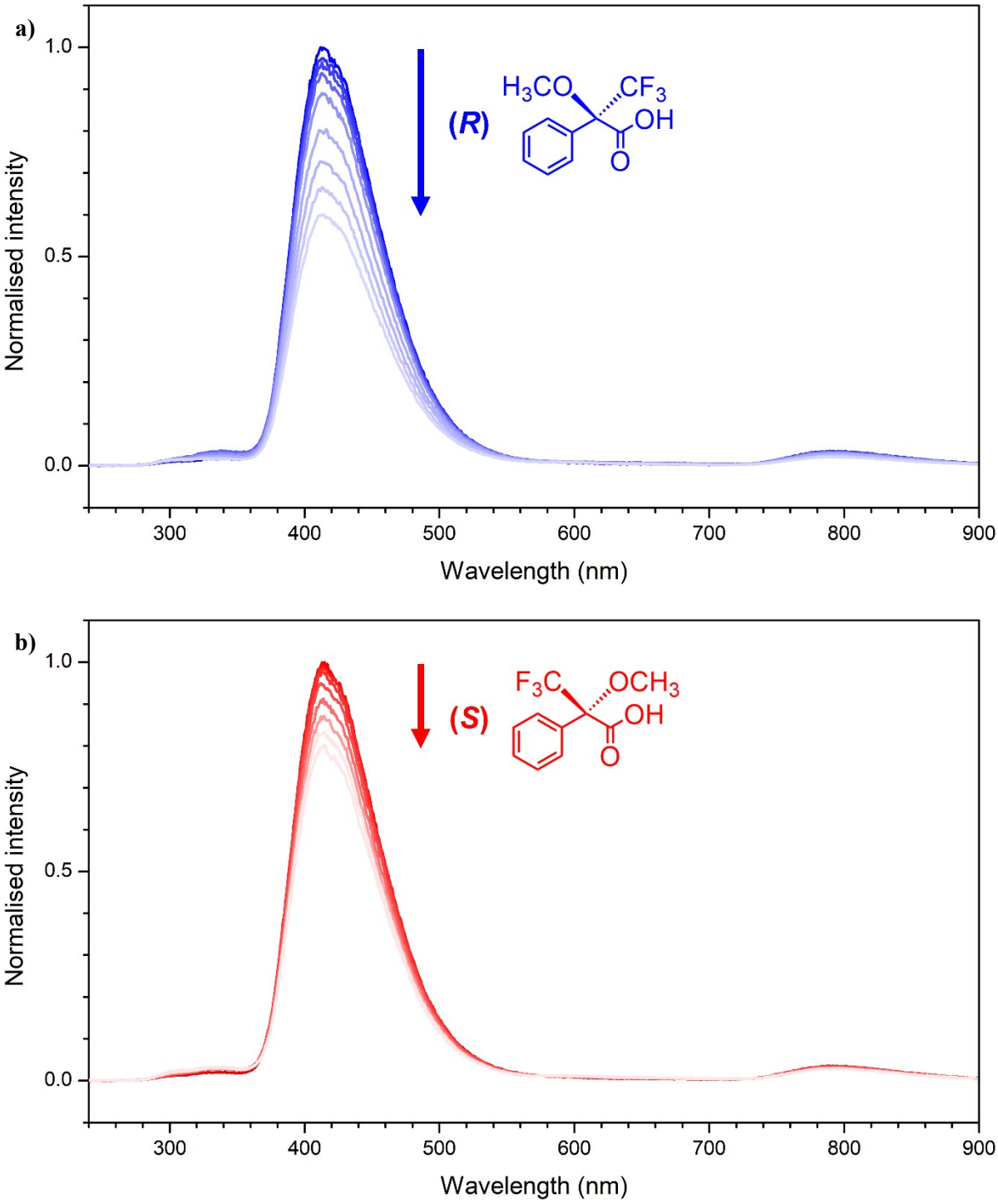

Figure S13. Normalised emission spectra of compound **(*S*)-1** as a suspension in acetonitrile after incremental additions (0–0.43 mM) of the enantiomers of chiral analyte **A**: a) (*R*)-Mosher's acid (blue); b) (*S*)-Mosher's acid (red). In both cases, excitation wavelength = 229 nm.

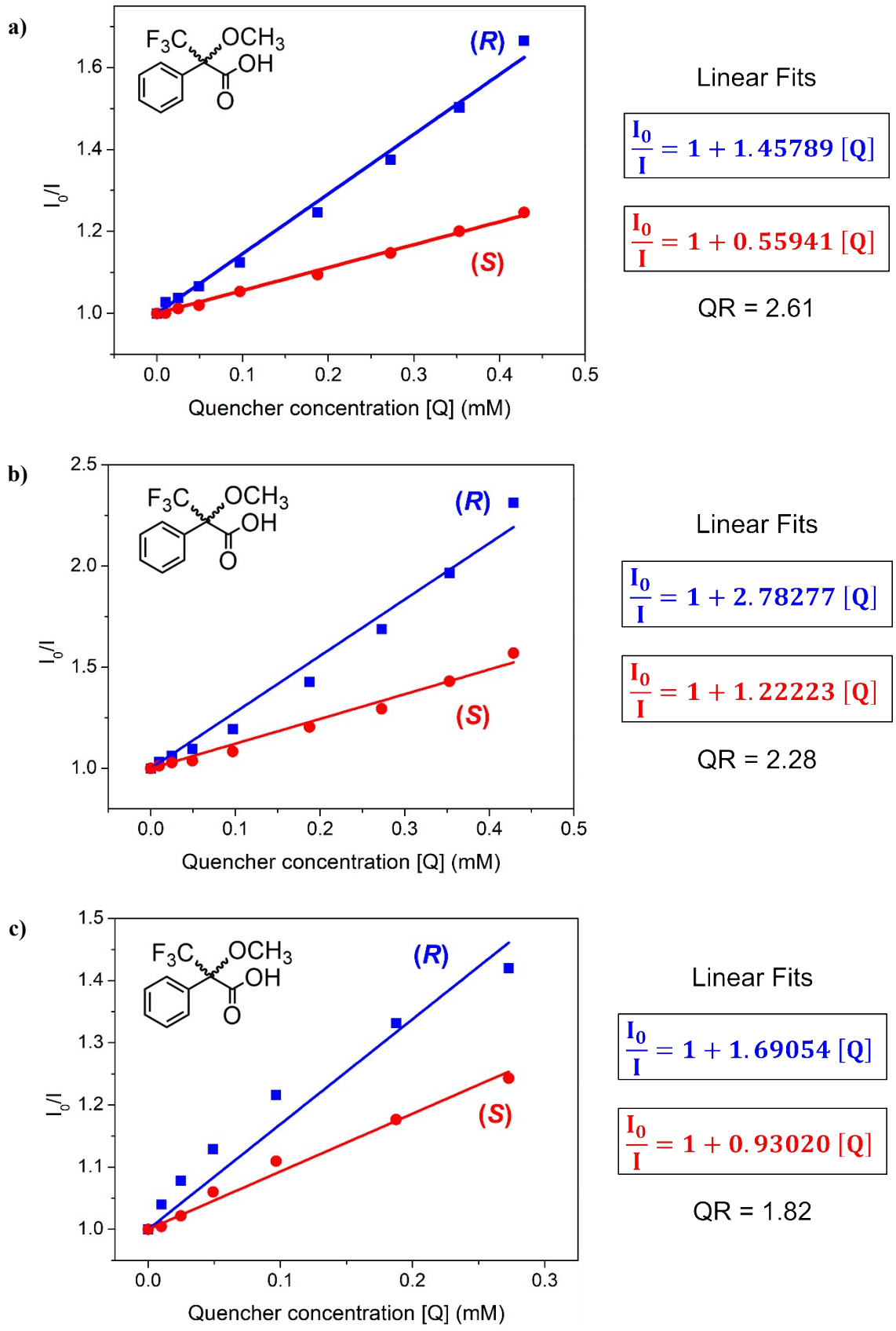

Figure S14. Stern-Volmer plots showing the quenching of compound **(*S*)-1** by the enantiomers of Mosher's acid (analyte **A**), used in the calculation of an average QR value of 2.23 (± 0.39). In all cases, linear fits for the (*R*)-enantiomer (blue) and (*S*)-enantiomer (red) are shown.

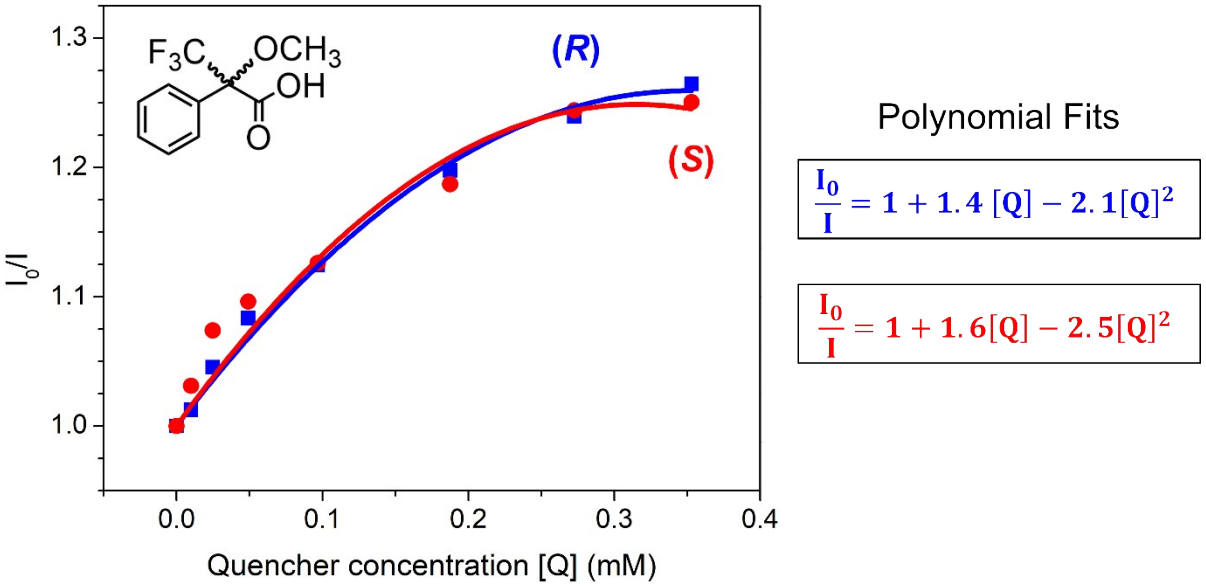

Figure S15. Curved Stern-Volmer plots showing the quenching of racemic compound **1** by the enantiomers of Mosher's acid (analyte **A**), conducted as a control experiment. These plots seem to curve towards an asymptote parallel with the *x*-axis before flattening. This negative curvature implies saturation of compound **1**'s binding sites,[7] possibly due to the lower CP concentration with which these measurements were taken. Nonetheless, equivalent responses were observed for both enantiomers of analyte **A**. Polynomial fits for the (*R*)-enantiomer (blue) and (*S*)-enantiomer (red) are shown.

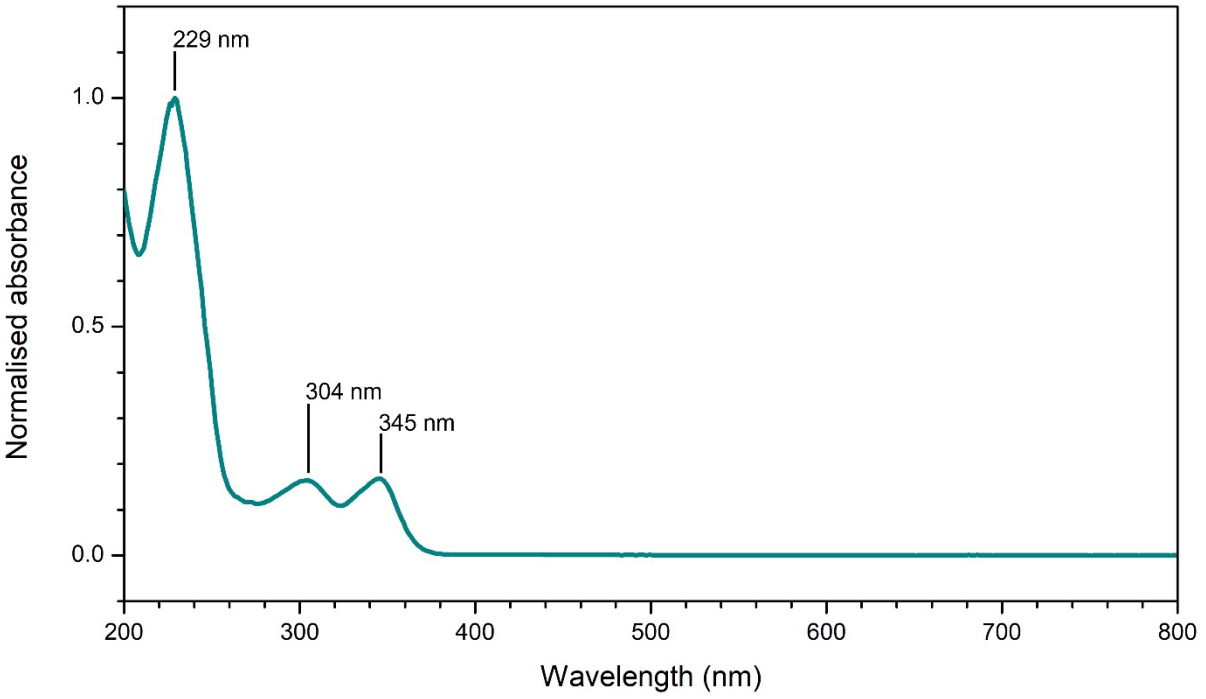

Figure S16. Normalised UV/vis absorption spectrum of ligand **L1** as an acetonitrile solution.

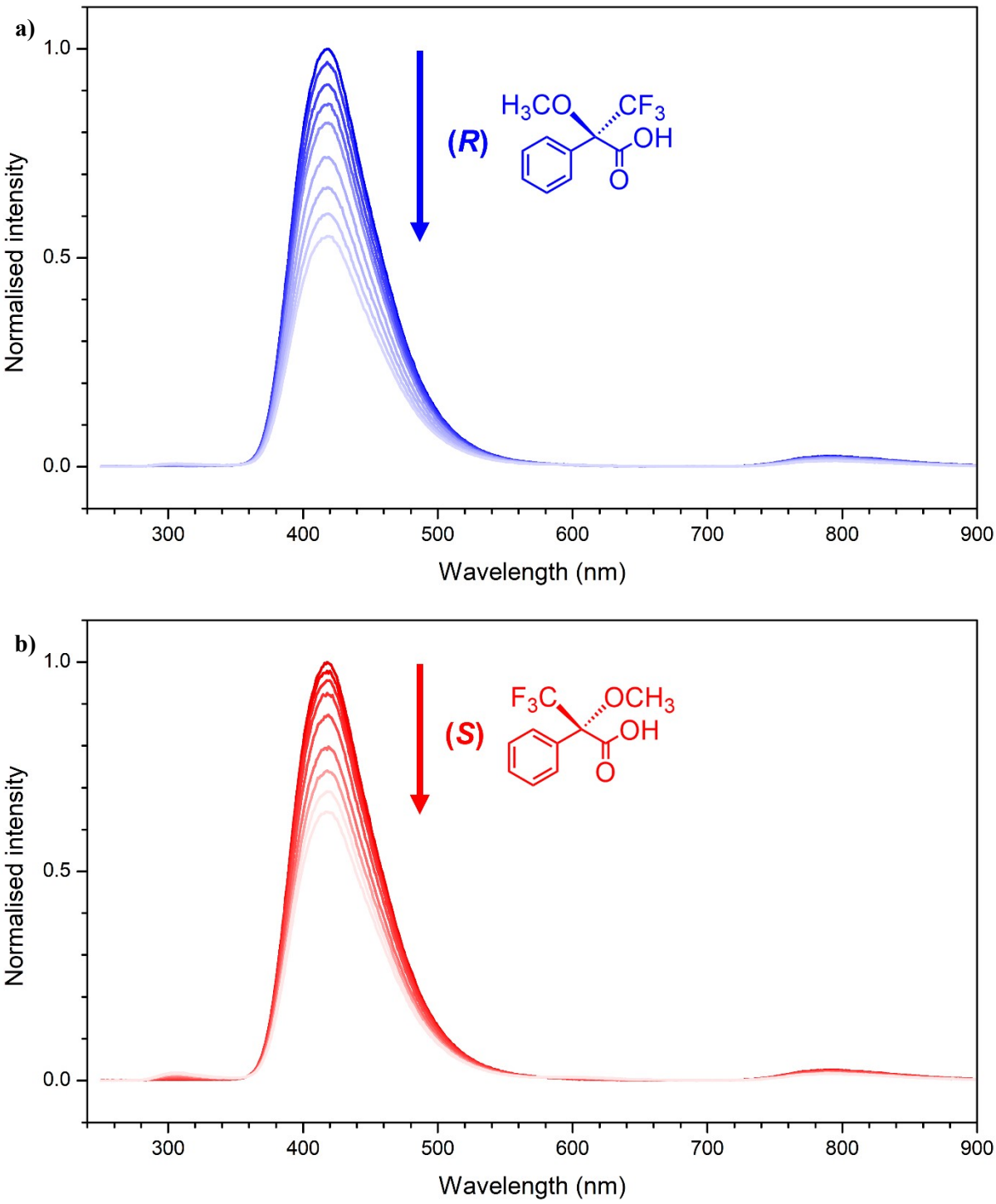

Figure S17. Normalised emission spectra of ligand **(*S*)-L1** as an acetonitrile solution after incremental additions (0–0.43 mM) of the enantiomers of chiral analyte **A**: a) (*R*)-Mosher's acid (blue); b) (*S*)-Mosher's acid (red). In both cases, excitation wavelength = 229 nm.

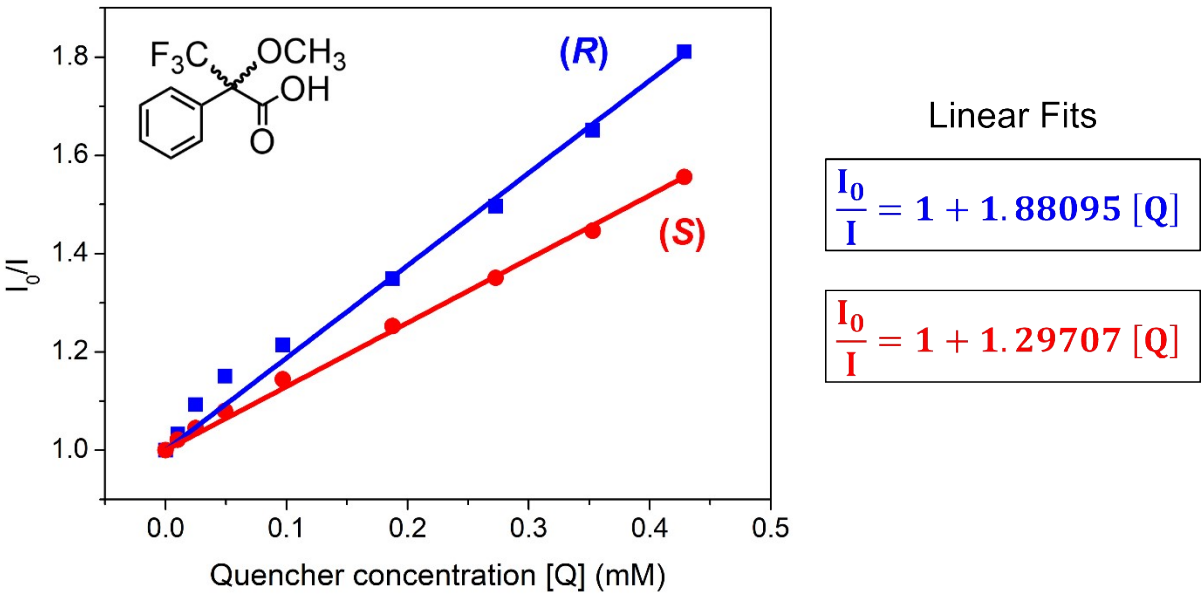

Figure S18. Stern-Volmer plots showing the quenching of ligand **(*S*)-L1** by the enantiomers of Mosher's acid (analyte **A**), conducted as a control experiment. Linear fits for the (*R*)-enantiomer (blue) and (*S*)-enantiomer (red) are shown. From these fits, a QR value of 1.45 was obtained, indicating that the **(*S*)-L1** ligand on its own is not as enantioselective as compound **(*S*)-1**.

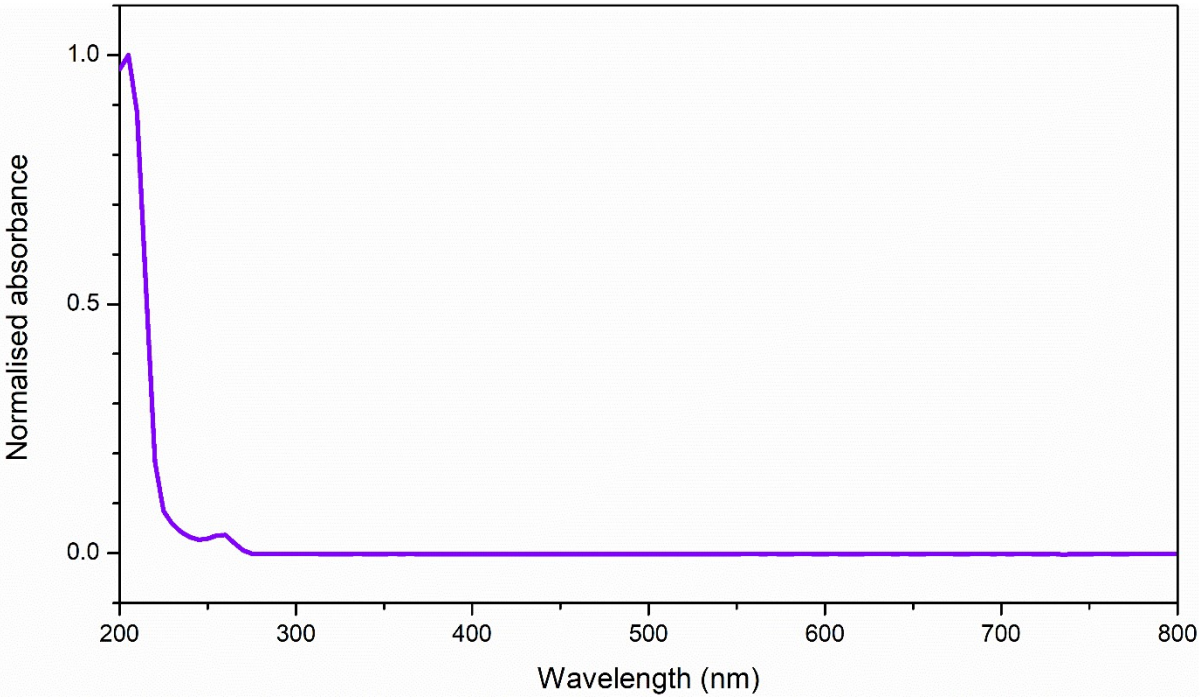

Figure S19. Normalised UV/vis absorption spectrum of Mosher's acid (chiral analyte **A**) as a solution in acetonitrile.

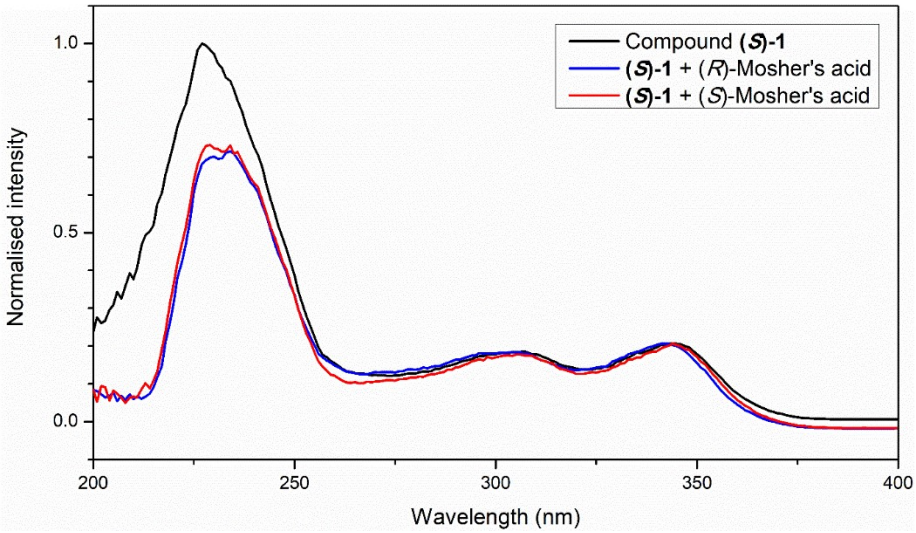

Figure S20. Normalised excitation spectra of compound **(*S*)-1** as a suspension in acetonitrile, monitoring emission at 415 nm. Spectra are shown for the suspension before (black) and after the addition of the enantiomers of analyte **A**: (*R*)-Mosher's acid (blue) and (*S*)-Mosher's acid. The decrease in intensity around 229 nm represents excitation light shielding by the analyte; however, the spectra for both enantiomers of Mosher's acid are equivalent, suggesting that the internal filter effect does not interfere with the enantioselectivity of compound **(*S*)-1**.

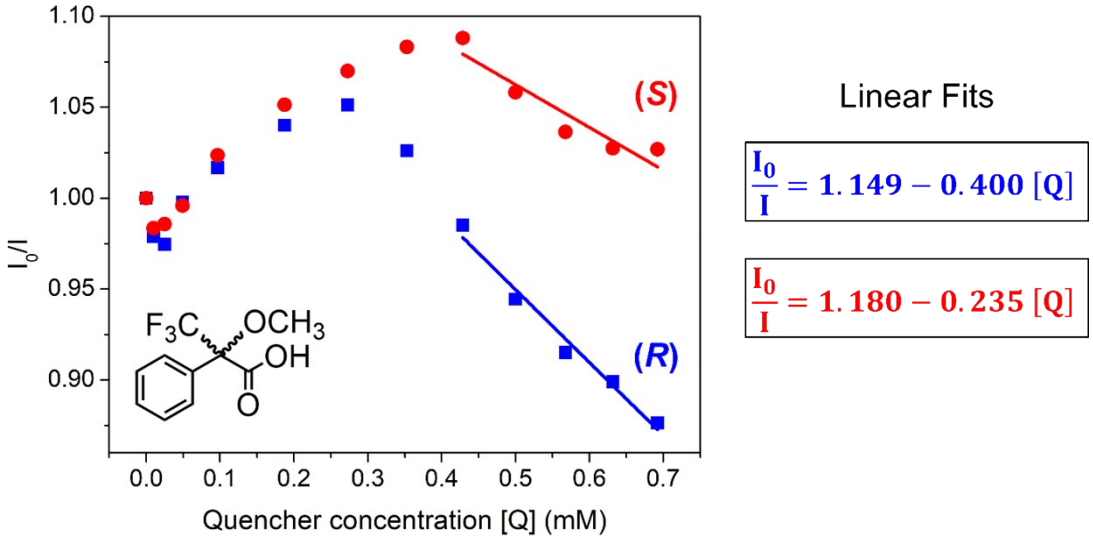

Figure S21. Stern-Volmer plots showing the quenching of compound **(*S*)-1** by the enantiomers of Mosher's acid (analyte **A**) upon excitation at 346 nm. Linear fits for the (*R*)-enantiomer (blue) and (*S*)-enantiomer (red) are shown for the fluorescence enhancement that occurs after 0.4 mM. The mechanism behind this enhancement is unknown.

From the approximate linear fits in these plots, a QR value of 1.71 was obtained, which is comparable to the enantioselectivity observed when exciting at 229 nm. Additionally, the fact that any quenching was observed when exciting at this wavelength suggests the excitation light shielding by Mosher's acid is not the only interaction causing quenching of the fluorescence of compound **(*S*)-1**.

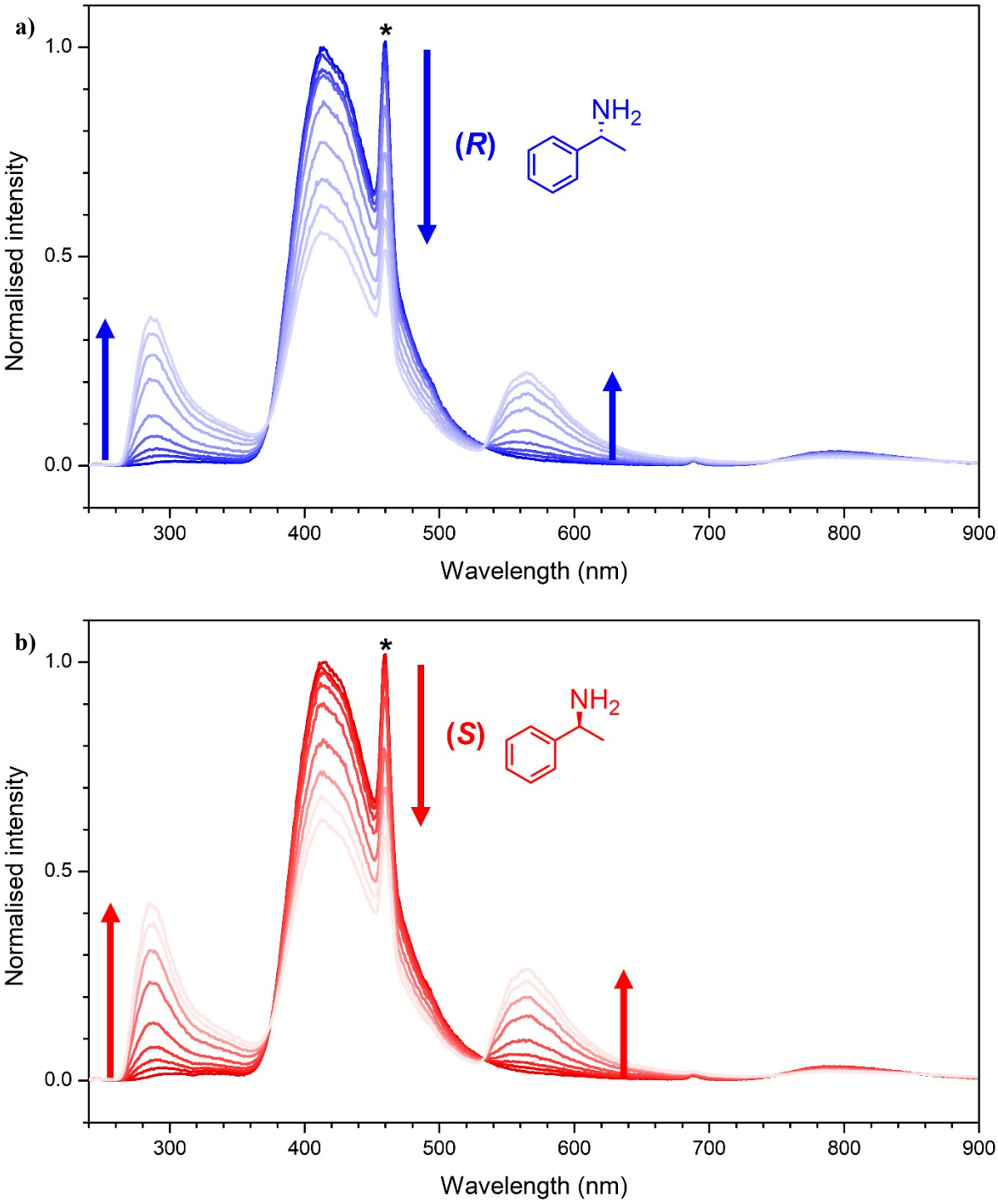

Figure S22. Normalised emission spectra of compound **(*S*)-1** as a suspension in acetonitrile after incremental additions (0–0.43 mM) of the enantiomers of chiral analyte **B**: a) (*R*)-1-phenylethylamine (blue); b) (*S*)-1-phenylethylamine (red). In both cases, excitation wavelength = 229 nm. The peaks related to the second harmonic is indicated with an asterisk. Additional peaks around 290 and 565 nm represent the increasing emission of the analyte itself.

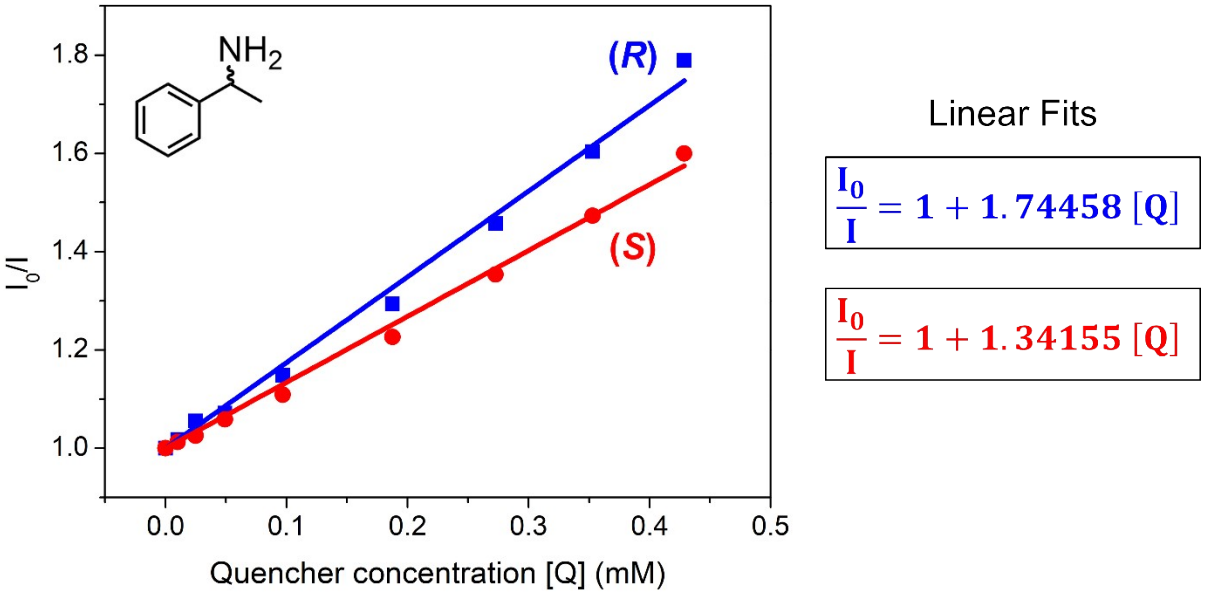

Figure S23. Stern-Volmer plots showing the quenching of compound **(*S*)-1** by the enantiomers of 1-phenylethylamine (analyte **B**). Linear fits for the (*R*)-enantiomer (blue) and (*S*)-enantiomer (red) are shown.

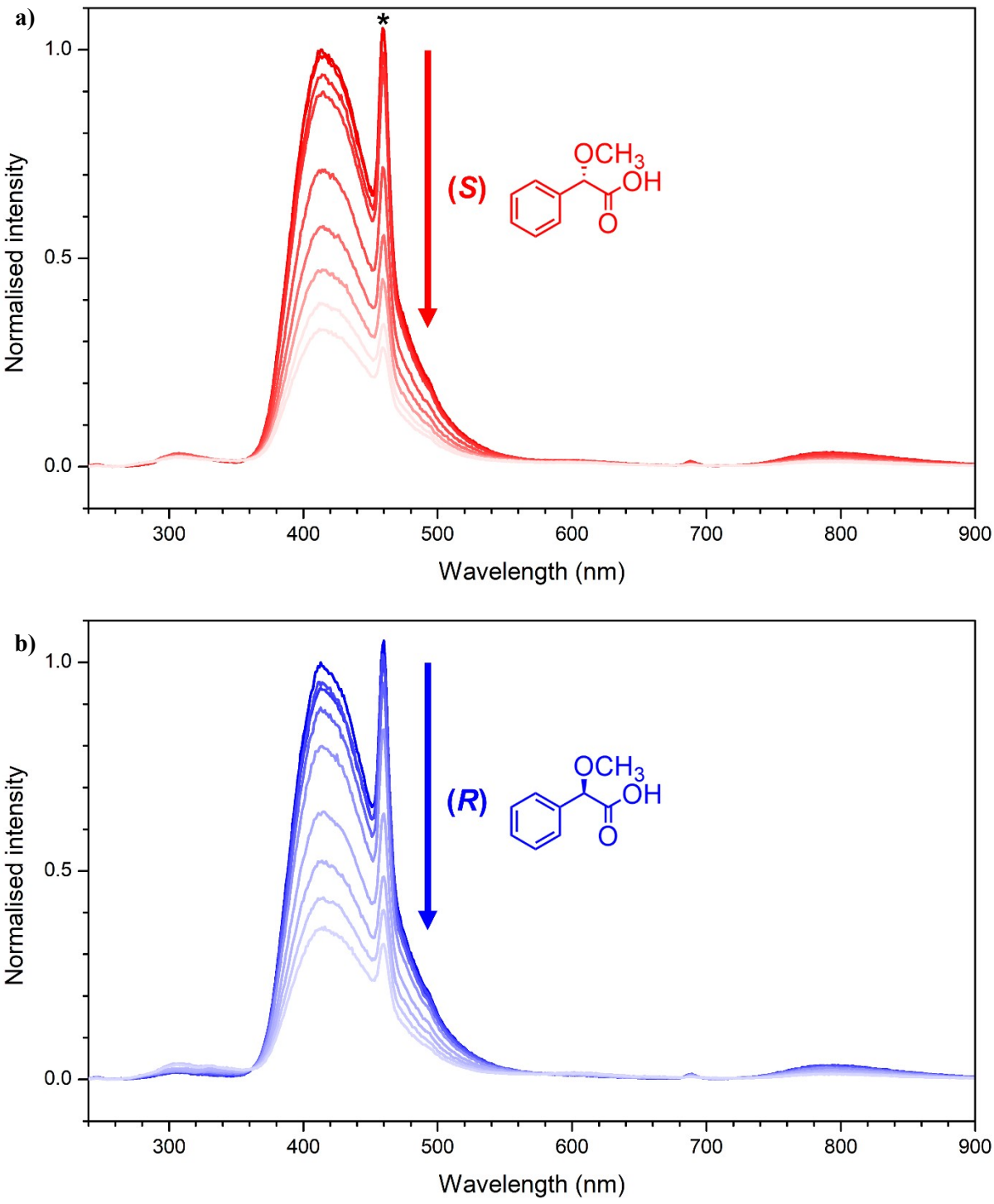

Figure S24. Normalised emission spectra of compound **(*S*)-1** as a suspension in acetonitrile after incremental additions (0–0.43 mM) of the enantiomers of α-methoxy-α-phenylacetic acid, analyte **C**: a) (*S*)-enantiomer (red); b) (*R*)-enantiomer (blue). In both cases, excitation wavelength = 229 nm. The peaks related to the second harmonic is indicated with an asterisk.

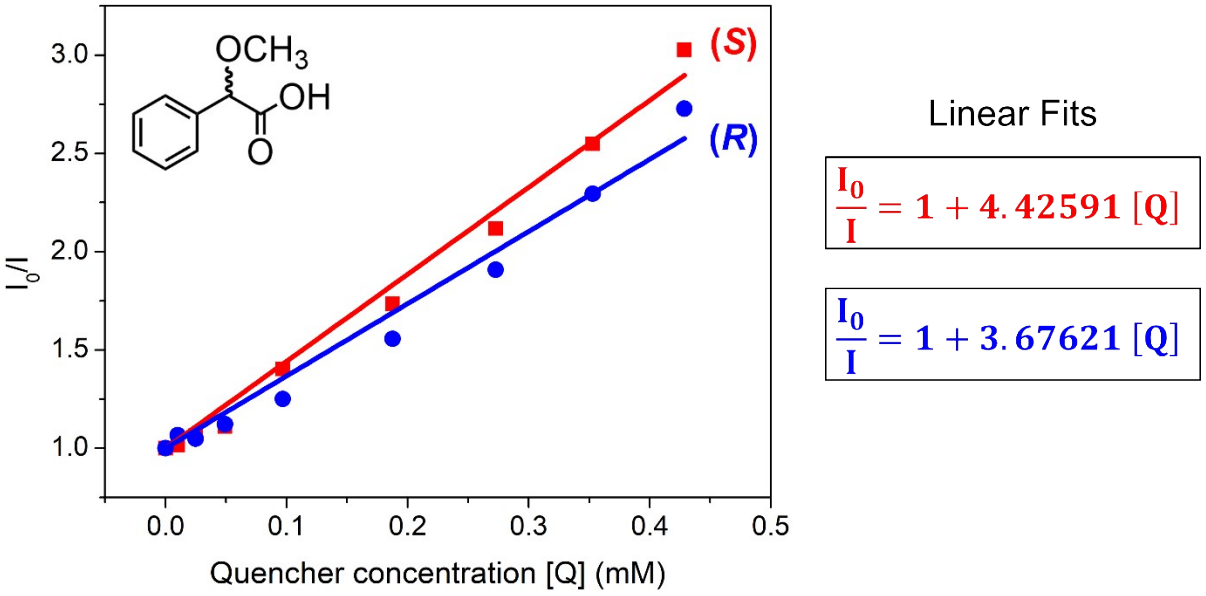

Figure S25. Stern-Volmer plots showing the quenching of compound **(*S*)-1** by the enantiomers of α-methoxy-α-phenylacetic acid (analyte **C**). Linear fits for the (*S*)-enantiomer (red) and (*R*)-enantiomer (blue) are shown.

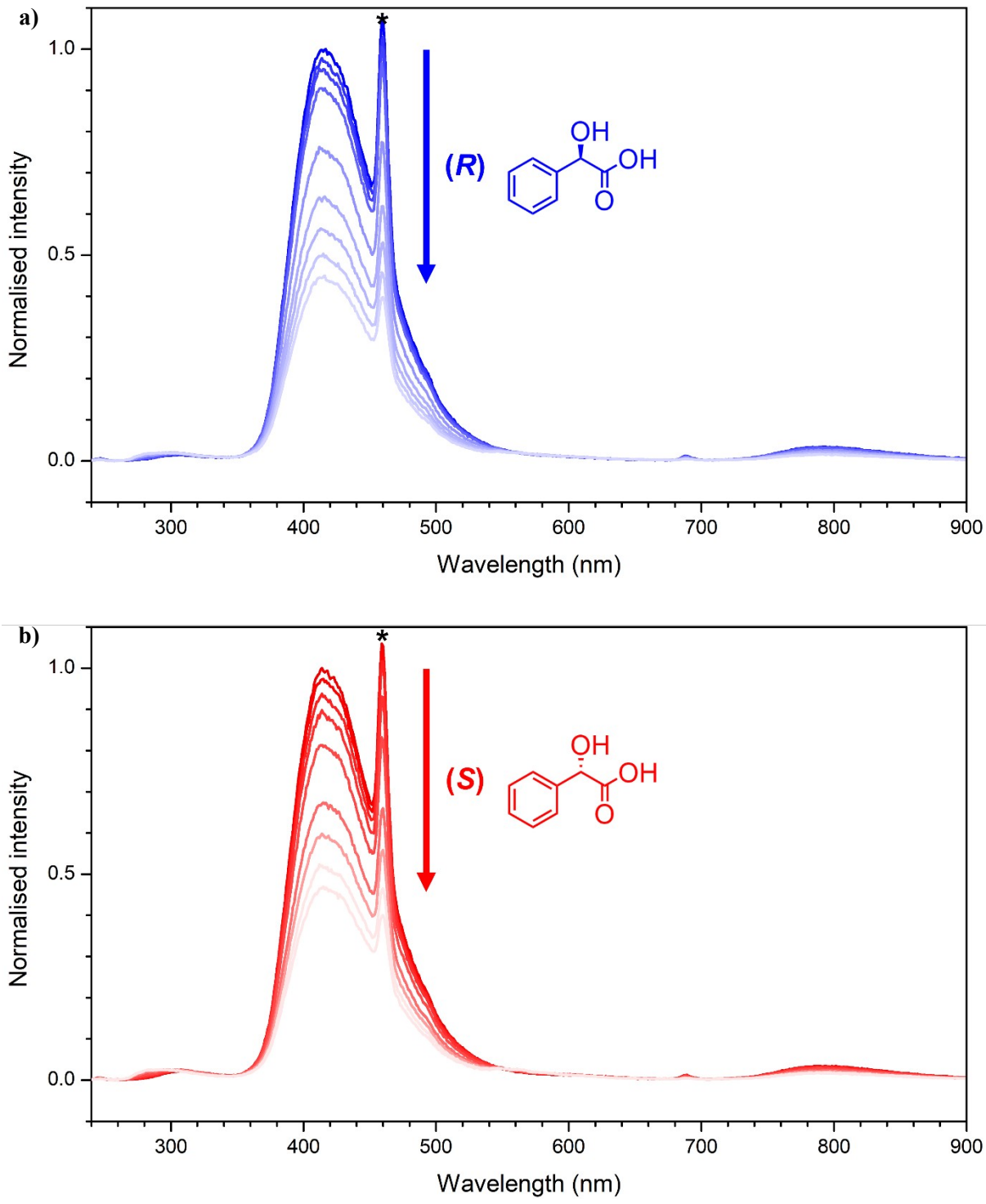

Figure S26. Normalised emission spectra of compound **(*S*)-1** as a suspension in acetonitrile after incremental additions (0–0.43 mM) of the enantiomers of chiral analyte **D**: a) (*R*)-mandelic acid (blue); b) (*S*)-mandelic acid (red). In both cases, excitation wavelength = 229 nm. The peaks related to the second harmonic is indicated with an asterisk.

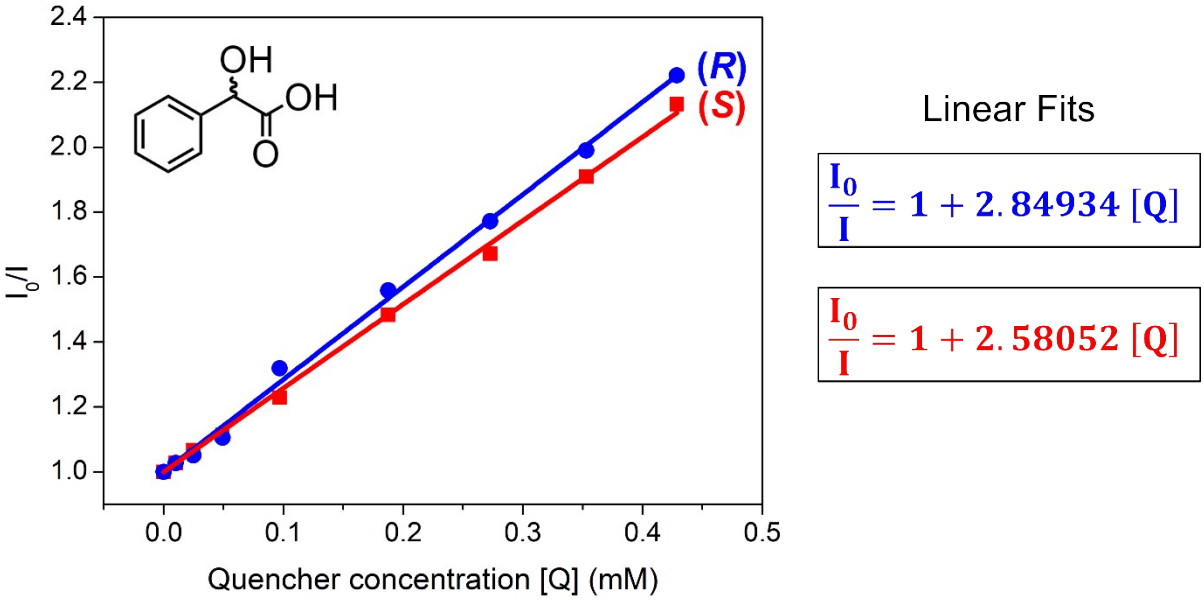

Figure S27. Stern-Volmer plots showing the quenching of compound **(*S*)-1** by the enantiomers of mandelic acid (analyte **D**). Linear fits for the (*R*)-enantiomer (blue) and (*S*)-enantiomer (red) are shown.

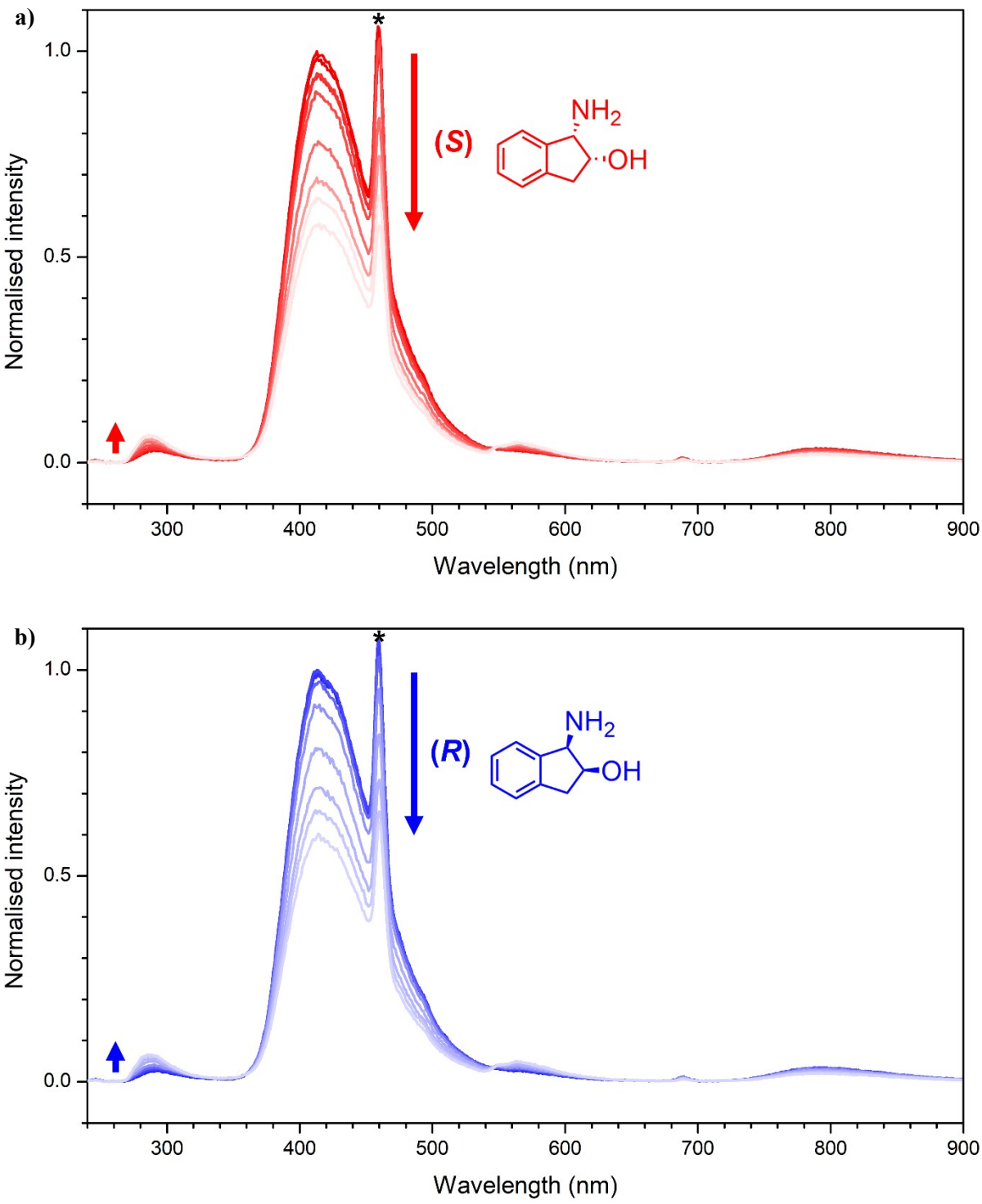

Figure S28. Normalised emission spectra of compound **(*S*)-1** as a suspension in acetonitrile after incremental additions (0–0.43 mM) of the enantiomers of *cis*-1-amino-2-indanol, chiral analyte **D**: a) (1*S*,2*R*)-enantiomer (red); b) (1*R*,2*S*)-1-phenylethylamine (blue). In both cases, excitation wavelength = 229 nm. The peaks related to the second harmonic is indicated with an asterisk. Additional peaks around 290 nm represent the increasing emission of the analyte itself.

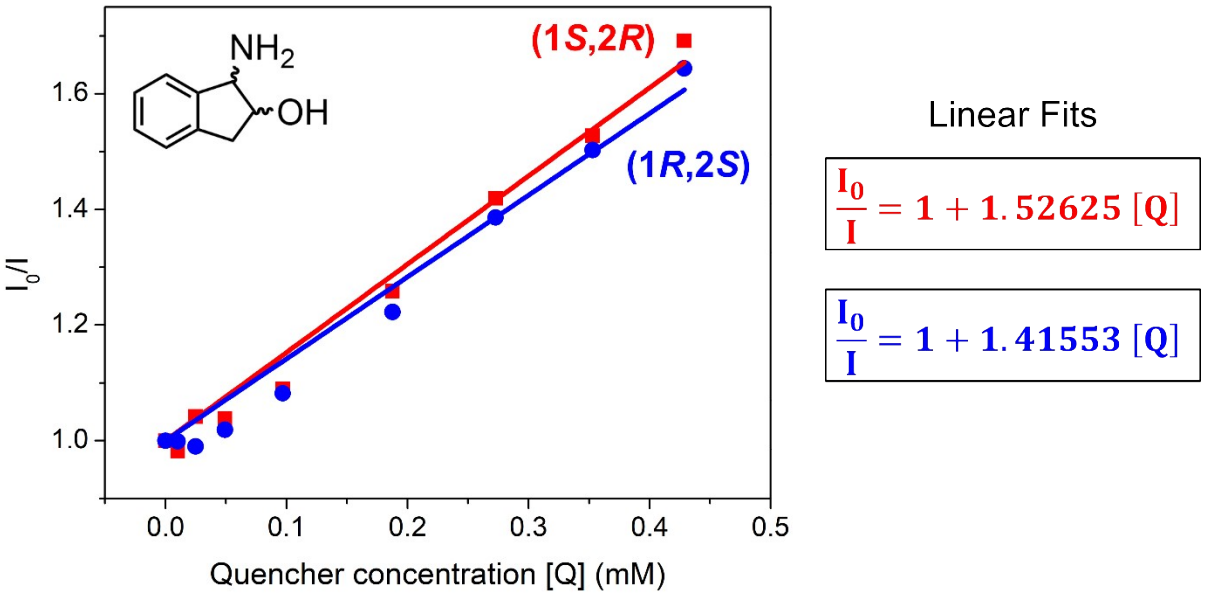

Figure S29. Stern-Volmer plots showing the quenching of compound **(*S*)-1** by the enantiomers of *cis*-1-amino-2-indanol (analyte **E**). Linear fits for the (1*S*,2*R*)-enantiomer (red) and (1*R*,2*S*)-enantiomer (blue) are shown.

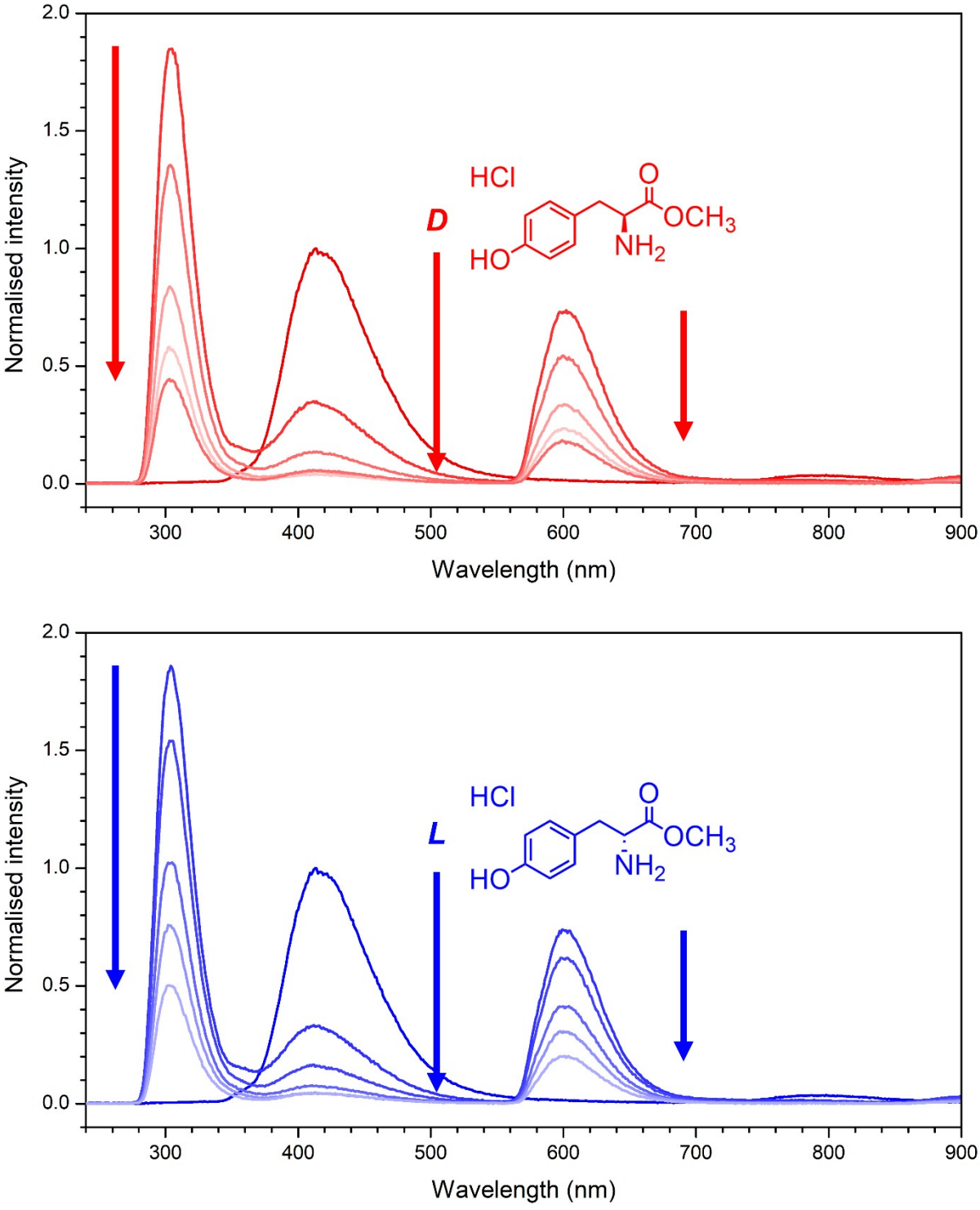

Figure S30. Normalised emission spectra of compound **(*S*)-1** as a suspension in acetonitrile after incremental additions (0–0.43 mM) of the enantiomers of tyrosine methyl ester, HCl: a) *D*-enantiomer (red); b) *L*-enantiomer (blue). In both cases, excitation wavelength = 229 nm. The peaks around 305 and 600 nm represent the emission of the analyte itself, which interestingly decreases as the analyte's concentration increases.

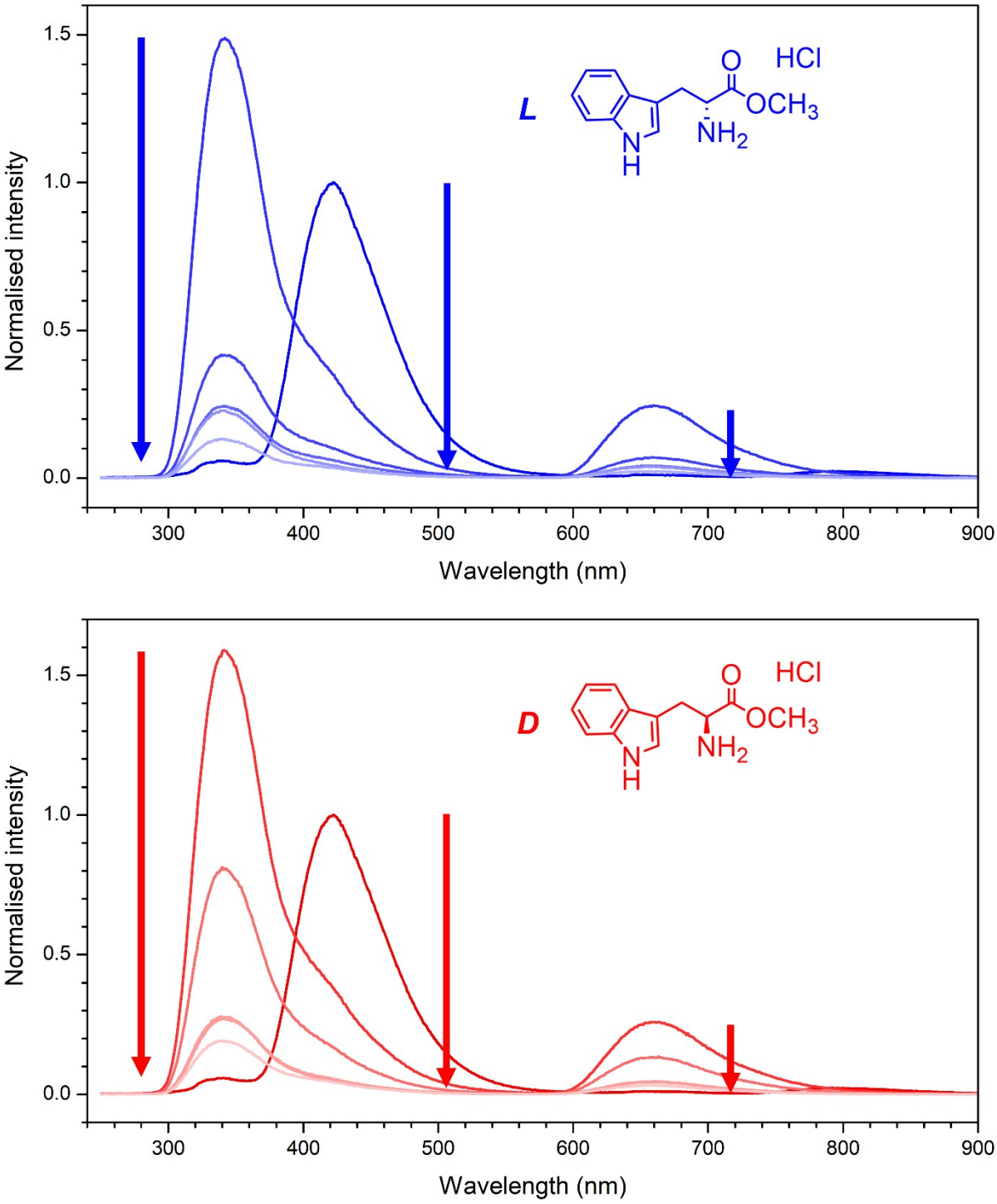

Figure S31. Normalised emission spectra of compound **(*S*)-1** as a suspension in acetonitrile after incremental additions (0–0.43 mM) of the enantiomers of tryptophan methyl ester, HCl: a) *L*-enantiomer (blue); b) *D*-enantiomer (red). In both cases, excitation wavelength = 229 nm. The peaks around 340 and 660 nm represent the emission of the analyte itself, which interestingly decreases as the analyte's concentration increases.

Mapping the quenching of compound **1** by the enantiomers of tryptophan methyl ester, HCl to the quadratic Stern-Volmer equation was not as successful as it was for tyrosine methyl ester, HCl in the main text. However, it was expected that pursuing further measurements would not be worthwhile, as the enantioselectivity shown by **1** for tryptophan methyl ester was not markedly different to that of tyrosine methyl ester.

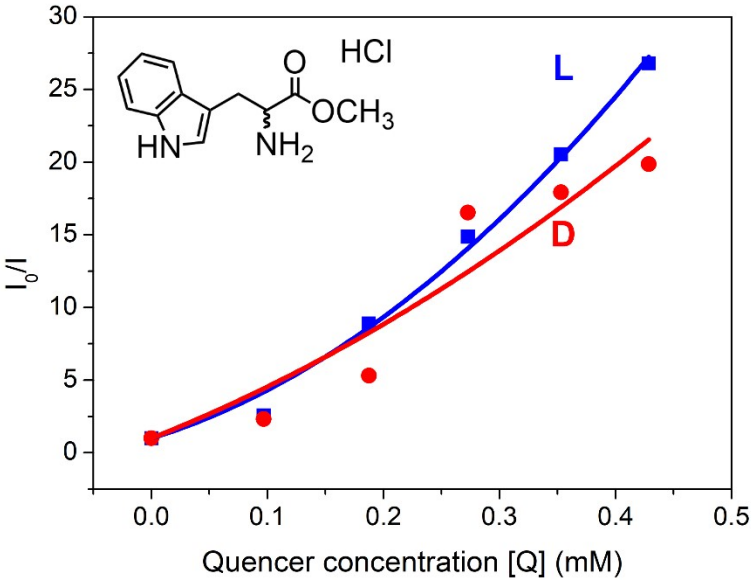

Polynomial Fits

$$\frac{I_0}{I} = 1 + 24.6[Q] + 85.4[Q]^2$$

$$\frac{I_0}{I} = 1 + 31.6[Q] + 38.1[Q]^2$$

Figure S32. Quadratic Stern-Volmer plots showing the quenching of compound **(*S*)-1** by the enantiomers of tryptophan methyl ester, HCl. Approximate polynomial fits for the *L*-enantiomer (blue) and *D*-enantiomer (red) are shown.

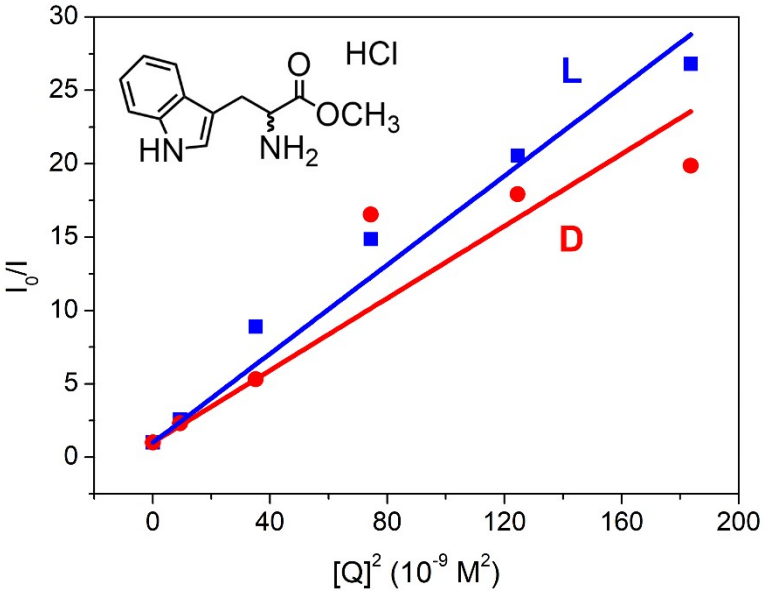

Linear Fits

$$\frac{I_0}{I} = 1 + 0.15145\,[Q]^2$$

$$\frac{I_0}{I} = 1 + 0.12289\,[Q]^2$$

Figure S33. Linear Stern-Volmer plots showing the quenching of compound **(*S*)-1** by the enantiomers of tryptophan methyl ester, HCl, with respect **[Q]²**. Linear fits for the *L*-enantiomer (blue) and *D*-enantiomer (red) are shown.

References

1. M. W. A. Maclean, T. K. Wood, G. Wu, R. P. Lemieux and C. M. Crudden, *Chem. Mater*., 2014, **26**, 5852.

2. S. Carrasco and B. Martín-Matute, *Eur. J. Inorg. Chem.*, 2019, **2019**, 1951.

3. N. P. Cowieson, D. Aragao, M. Clift, D. J. Ericsson, C. Gee, S. J. Harrop, N. Mudie, S. Panjikar, J. R. Price, A. Riboldi-Tunnicliffe, R. Williamson and T. Caradoc-Davies, *J. Synchrotron Radiat.*, 2015, **22**, 187.

4. G. M. Sheldrick, *Acta Crystallogr. Sect. A Found. Adv.*, 2015, **71**, 3.

5. G. M. Sheldrick, *Acta Crystallogr. Sect. C Struct. Chem.*, 2015, **71**, 3.

6. O. V. Dolomanov, L. J. Bourhis, R. J. Gildea, J. A. K. Howard and H. Puschmann, *J. Appl. Crystallogr.*, 2009, **42**, 339.

7. M. Toprak, *Spectrochim. Acta – Part A Mol. Biomol. Spectrosc.*, 2016, **154**, 108.